iScience

Article

Roles of class III phosphatidylinositol 3-kinase, Vps34, in phagocytosis, autophagy, and endocytosis in retinal pigmented epithelium

Graphical abstract

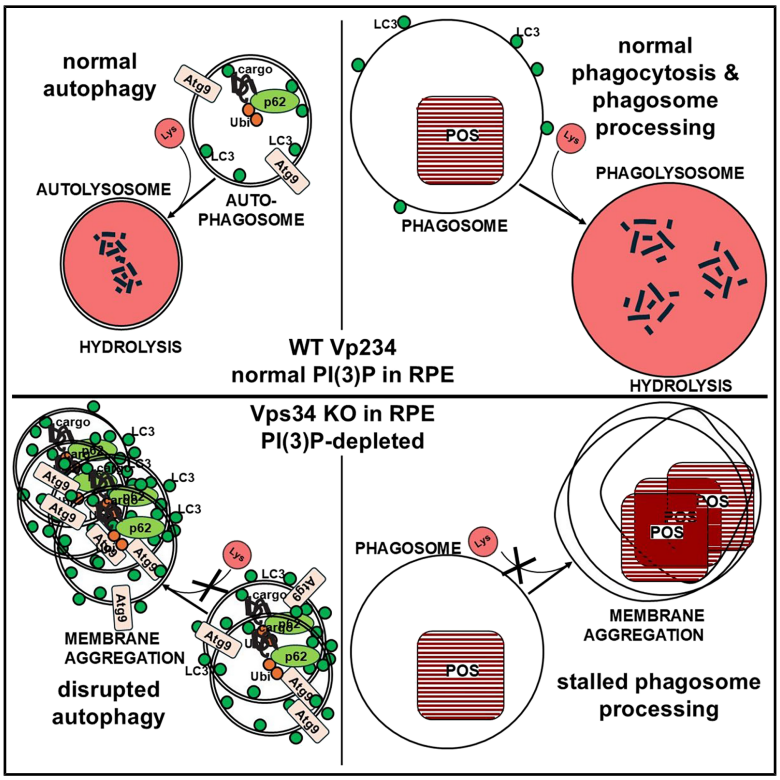

Highlights

- Vps34-derived PI(3)P needed to recruit LC3 to phagosomes and trigger lysosome fusion
- PI(3)P not needed to recruit LC3 to membranes with Atg9, Atg16L, ubiquitin, and p62
- PI(3)P not required to initiate phagocytosis of photoreceptor outer segment tips
- PI(3)P required for lysosomal degradation of autophagosomes, endosomes, and phagosomes

Authors

Feng He, Ralph M. Nichols, Melina A. Agosto, Theodore G. Wensel

Correspondence

twensel@bcm.edu

In brief

Enzymology; Lipid; Membranes; Functional aspects of cell biology; Model organism

He et al., 2025, iScience *28*, 112371
May 16, 2025
https://doi.org/10.1016/j.isci.2025.112371

CellPress

iScience

CellPress
OPEN ACCESS

Article

Roles of class III phosphatidylinositol 3-kinase, Vps34, in phagocytosis, autophagy, and endocytosis in retinal pigmented epithelium

Feng He,[1] Ralph M. Nichols,[2] Melina A. Agosto,[3] and Theodore G. Wensel[1,4,*]
[1]Department of Biochemistry and Molecular Pharmacology, Baylor College of Medicine, Houston, TX, USA
[2]Department of Ophthalmology, Baylor College of Medicine, Houston, TX, USA
[3]Retina and Optic Nerve Research Laboratory, Department of Physiology and Biophysics, and Department of Ophthalmology and Visual Sciences, Dalhousie University, Halifax, NS, Canada
[4]Lead contact
*Correspondence: twensel@bcm.edu
https://doi.org/10.1016/j.isci.2025.112371

SUMMARY

Phosphatidylinositol-3-phosphate (PI(3)P) is important for multiple functions of retinal pigmented epithelial (RPE) cells, but its functions in RPE have not been studied. In RPE from mouse eyes and in cultured human RPE cells, PI(3)P-enriched membranes include endosomes, the *trans*-Golgi network, phagosomes, and autophagophores. Mouse RPE cells lacking activity of the PI-3 kinase, Vps34, lack detectable PI(3)P and die prematurely. Phagosomes containing rod discs accumulate, as do membrane aggregates positive for autophagosome markers. These autophagy-related membranes recruit LC3/Atg8 without Vps34, but phagosomes do not. Vps34 loss leads to accumulation of lysosomes which do not fuse with phagosomes or membranes with autophagy markers. Thus, Vps34-derived PI(3)P is not needed for initiation of phagocytosis or endocytosis, nor for formation of membranes containing autophagy markers. In contrast, Vps34 and PI(3)P are essential for intermediate and later stages, including membrane fusion with lysosomes.

INTRODUCTION

The low-abundance phospholipid, phosphatidylinositol-3-phosphate (PI(3)P), plays important roles in membrane traffic within eukaryotic organisms. Its addition to membranes through the action of a protein complex containing the catalytic subunit Vps34 has been implicated in initiation of autophagy[1–3] and in processing of endosomes[4,5] and of phagosomes.[6] It also serves as the precursor for another membrane-targeting phosphoinositide, phosphatidylinositol-3,5-bisphosphate ($PI(3,5)P_2$), essential for completion of the degradation of these organelles by lysosomes.[7–9]

The retinal pigmented epithelium (RPE) is an epithelial layer immediately adjacent to the photoreceptor layer of the vertebrate retina, in which all three of these membrane-trafficking pathways are essential for its function and for vision. The RPE plays a critical role in maintaining the health of the rod and cone photoreceptors. The distal portions of light-sensing photoreceptor outer segments (POS) are embedded in apical processes of the RPE. When the retina is exposed to light there is a continual flux into the RPE of the vitamin-A-derivative, all-*trans*-retinol, generated as a by-product of vision in the POS. This inward flow is balanced by a return flux of the visual pigment, 11-*cis*-retinaldehyde, generated by visual cycle enzymes, including the isomerohydrolase, RPE65, in the RPE.[10–12] A distinct process for continual renewal of outer segment contents occurs through phagocytosis of the distal tips of POS by the RPE.[13–16] Endocytosis is also an important function in RPE[17,18] for taking up nutrients and capturing all-*trans*-retinol bound to interstitial retinol binding protein (IRBP),[19] although RPE endocytosis has been less extensively studied than phagocytosis or autophagy. In recent years, the role in the RPE of autophagy, the program for digestion of self-derived cellular components for renewal and nutrient provision, has received considerable attention,[20] accompanied by suggestions that deficiencies in autophagy may play a role in the major blinding disease of the elderly, age-related macular degeneration (AMD).[21]

Whereas PI(3)P plays critical roles in trafficking of endosomes and autophagosomes generally, phagocytosis of POS by RPE is a more specialized process, in which the role of PI(3)P has not been extensively explored. In particular, POS phagocytosis involves a mechanism known as LC3-associated phagocytosis (LAP), in which the ubiquitin-like protein LC3 (Atg8 in *Saccharomyces cerevisiae*) is recruited to membranes and covalently attached via an amide linkage to phosphatidylethanolamine, forming the lipid-modified form, LC3-II from the soluble form, LC3-I. Recruitment of LC3-II is a well-established step in autophagosome maturation, with LC3 serving to capture the adaptor protein, p62, which in turn binds to ubiquitinated cargo destined for lysosomal degradation. LC3-II also facilitates transport to lysosomes through interactions with microtubule motor and motor-adaptor proteins.[22–24]

Marking of phagophore membranes with PI(3)P is an early step in autophagy, catalyzed by a Vps34-containing protein complex I that also contains Vps15, Beclin 1, AMBRA1, and ATG14L.[25,26] Although this mechanism is well established, there are alternative mechanisms for generating LC3-II-containing autophagy-related membranes in the absence of Vps34 and its synthesis of PI(3)P. In mouse cells lacking Vps34 due to conditional knockouts, unprocessed membrane aggregates containing LC3-II, Atg9, p62, and ubiquitinated cargo accumulate, along with large numbers of enlarged lysosomes, with which they do not fuse.[27–32]

The role of PI(3)P in RPE LAP is less clear. In other cell types a Vps34 complex of distinct composition (UVRAG and Rubicon substituted for AMBRA1 and ATG14L) catalyzes formation of PI(3)P on phagosomes, and PI(3)P appears to be needed for progression of phagosome processing, but not for phagocytic cup formation or engulfment.[33] Whether PI(3)P-binding early endosome protein EEA1 is recruited to RPE phagosomes has not been determined, nor has a role for LC3-binding autophagy adaptor protein, p62, been reported for RPE phagocytosis.

In order to determine the role of PI(3)P and Vps34 in LAP within RPE and to understand the interplay among roles for PI(3)P in endocytosis, autophagy and phagocytosis, we determined localization of PI(3)P in RPE cells in culture and *in vivo* and developed a mouse strain with conditional knockout within the RPE of the catalytic functionality of Vps34. We further bred these mice with an existing strain whose rod outer segments are filled with rhodopsin bearing an EGFP fusion for facile identification of POS phagosomes.

RESULTS

Localization of PI(3)P in cultured human RPE cells

To determine the localization of PI(3)P in RPE cells, we expressed a protein construct with two copies of the PI(3)P-binding domain of Hrs fused to enhanced green fluorescent protein (GFP-2xHrs) as described previously.[29] This construct allows the visualization of PI(3)P membranes as bright puncta in cells. In the immortalized human cell line, ARPE-19, in healthy cells (Figure 1), numerous puncta of PI(3)P were observed, ranging in size from near the diffraction limit ($\leq$300 nm) to $\sim$2 μm, which were confirmed in control experiments to be missing in cells treated with the Vps34 inhibitor, Vps34-IN1 (Figure S1A). In live-cell imaging experiments, PI(3)P puncta disappeared on a timescale of minutes upon addition of Vps34-IN1 (Figure S1A), but were stable on that timescale when vehicle was added (Figure S1B) verifying Vps34 as the major enzyme producing the PI(3)P in these puncta. These puncta did not co-localize with two markers of the endoplasmic reticulum, Sec61 and BiP, nor with the *cis*-Golgi marker, GM130 (Figures 1A–1C). Many of them did, however, colocalize strongly with the *trans*-Golgi marker TGN46 (Figure 1D). While there was extensive overlap of PI(3)P with the *trans*-Golgi, some PI(3)P-labeled puncta did not co-localize with TGN46, and many TGN46 puncta did not display PI(3)P labeling, suggesting at least three distinct subcompartments labeled with one or both of these probes. These results contrast with previous reports from other cell types, in which virtually no co-localization of PI(3)P with a *trans*-Golgi marker was observed.[34] A subset of PI(3)P puncta co-localized with either early endosome marker, Rab5 (Figure 1E), or late endosome marker, Rab7 (Figure 1F). These results indicate that there are multiple pools of PI(3)P-containing membranes in ARPE-19 cells, even when two processes known to rely on PI(3)P, phagocytosis and autophagy, are only at basal levels, with no detectable accumulation of membranes associated with these processes.

To enhance the level of observable autophagosomes, we treated cells with chloroquine which inhibits lysosome acidification and blocks the fusion of autophagosomes with lysosomes and subsequent degradation. Under these conditions, there is a massive accumulation of puncta positive for autophagy marker LC3/Atg8 (Figures 2A–2D and 2H–2L), which also contain the autophagy markers p62, Atg16L, and Atg9 (Figures 2E–2H). *Arrows* indicate puncta visible in more than one channel for alignment and comparison in adjacent panels. In most samples, the putative PI(3)P-binding protein WIPI2/Atg18[35] also co-localized with LC3, p62, and Atg16L puncta (Figures 2C, 2E, and 2F), although we have occasionally observed samples where there was little, if any, overlap of LC3 and WIPI2 signal. The LC3 puncta are surrounded by, but not truly co-localized with, 2XHrs signal (Figure 2B). Most of the GFP-2xHrs signal was observed in large, aggregated membranes surrounding central cavities that were unlabeled. In most, but not all, of these PI(3)P-containing structures, the central cavity was strongly labeled by LC3. The WIPI2 spatial distribution (Figures 2C, 2E, and 2F) is distinct from the pattern displayed by 2XHrs, coinciding with the LC3 signal rather than surrounding it as the PI(3)P signal does (Figure 2B). WIPI1 signal (Figure 2D) resembled that for WIPI2.

Vps34-containing complexes are known to play an important role in initiation of autophagy in multiple cell types, although the early stages of autophagy can still occur in the absence of Vps34 catalytic activity[36] or of PI(3)P.[27–32] In the chloroquine-treated cells there were also multiple large LC3-marked aggregates lacking PI(3)P signal, possibly as a result of conversion of PI(3)P to PI(3,5)P_2, a known step in autophagosome maturation catalyzed by PIKFYVE.[37] LC3 did not co-localize with markers for PI(4)P (GFP-2xFAPP1), PI(5)P (DsRed-3xING2), or PI(3,4)P_2 (DsRed-2xTAPP1) (Figures 2I, 2J, and 2K). Signal for the PI(4,5)P_2 marker, GFP-PLCδ, did correlate with LC3 signal (Figure 2G), surrounding it much like the PI(3)P signal (Figure 2L).

To determine the role of Vps34 and PI(3)P in phagocytosis in these cells, we fed them rod POS isolated from retinas of mice with a single copy of a knockin allele at the *Rhodopsin* locus, encoding human rhodopsin fused at its C-terminus to EGFP (hRho-GFP, referred to here as "**RG**"[38,39] [To simplify the nomenclature and allow more concise labeling of figures, we employ the following designations for each of the mouse genotypes studied, all bred onto a C57Bl6/J (C57BL/6J, B6 albino (B6(Cg)-Tyrc-2J/J) background:**ΔRPE** (knockout of *Vps34* in RPE) : *Vps34*$^{fl/fl}$/*Tg(BEST1-cre)Jdun*+/-; **WT** (no floxed allele or Cre transgene): *Vps34*$^{+/+}$/*Tg(BEST1-cre)Jdun*-/-; **Cre** (Cre transgene with homozygous WT *Vps34*): *Vps34*$^{+/+}$/*Tg(BEST1-cre)Jdun*+/-; **Cre/Fl/+** (*Cre*+/*Vps34*het): *Vps34*$^{fl/+}$/*Tg(BEST1-cre)Jdun*+/-; **Cre/+/+** (*Cre*+/*Vps34*WT): *Vps34*$^{+/+}$/*Tg(BEST1-cre)Jdun*+/-; **Fl/+** (*Vps34*het, no Cre): *Vps34*$^{+/fl}$/*Tg(BEST1-cre)Jdun*-/-; **Fl/Fl** (*Vps34* homozygous floxed, no Cre): *Vps34*$^{fl/fl}$/*Tg(BEST1-cre)Jdun*-/-. When

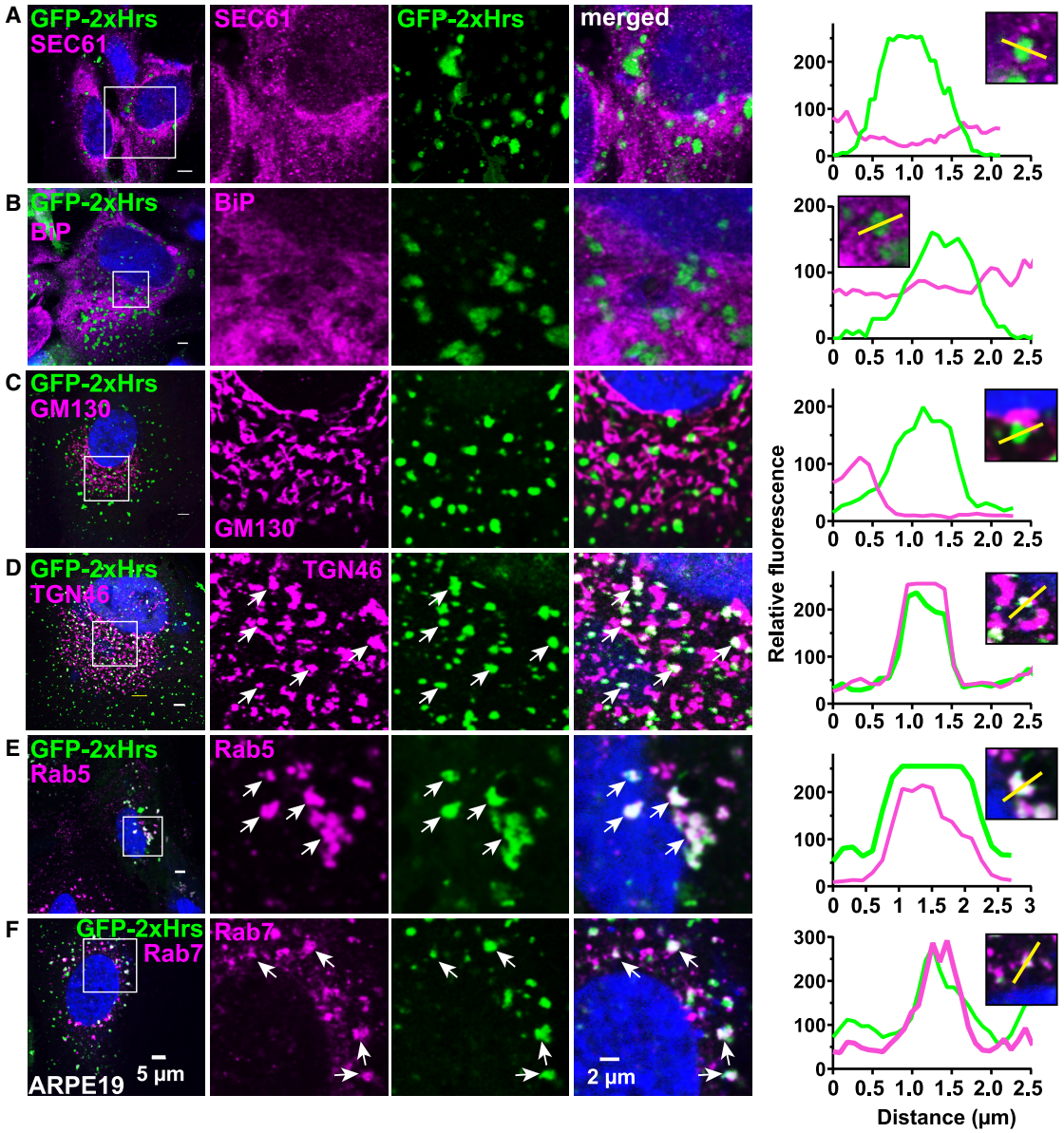

Figure 1. Localization of PI(3)P in cultured RPE cells

(A–F) ARPE-19 cells were transfected with plasmid directing expression of GFP-2xHrs probe and stained with antibodies directed against the indicated antigens. *Left* panels show low-magnification images (scale bars, 5 µm) and right panels show the boxed areas from left panels at higher magnification (scale bars, 2 µm). Line profiles of indicated puncta are plotted on far right for GFP-2xHrs (*green*) and indicated antigens (*magenta*). Antigens were selected as markers for endoplasmic reticulum (A, sec61 and B, BiP), *cis*-Golgi (C, GM130), *trans*-Golgi network (D, TGN46) or endosomal compartment (E, Rab5, early endosomes, F, Rab7, late endosomes). Arrows indicate PI(3)P-positive puncta also positive for TGN46 (D), Rab5 (E), or Rab7 (F).

the genotype includes the human rhodopsin-EGFP knockin at the *Rho* locus, "**/RG**" is appended to the end of the genotype designation, *e.g.*, **ΔRPE/RG** = *Vps34*$^{fl/fl}$/*Tg(BEST1-cre)Jdun*$^{+/-}$/*Rho*$^{hrhoG(H)/+}$. Note that only **ΔRPE and ΔRPE/RG** are missing Vps34 catalytic activity in Cre-expressing cells.]) (Figures 3A–3D; *arrows* denote puncta expanded in high-magnification *insets*). The phagocytosed POS were readily visualized by EGFP fluorescence after loose POS were washed from the surface, and these were surrounded by membranes staining strongly with an antibody specific for LC3. Virtually all the EGFP-labeled POS in the ARPE-19 culture with active Vps34 were labeled by LC3 (Figures 3A and C), indicating that the POS that remained after washing had been phagocytosed and were not merely adhering to the cell surface. Addition of Vps34 inhibitor, VPS34-IN1, eliminated the LC3 signal on the phagosomes (Figures 3B and 3D). When the cells were treated with the Vps34 inhibitor, phagocytosis still occurred (i.e., POS were visible after the washing procedure), but the phagosomes

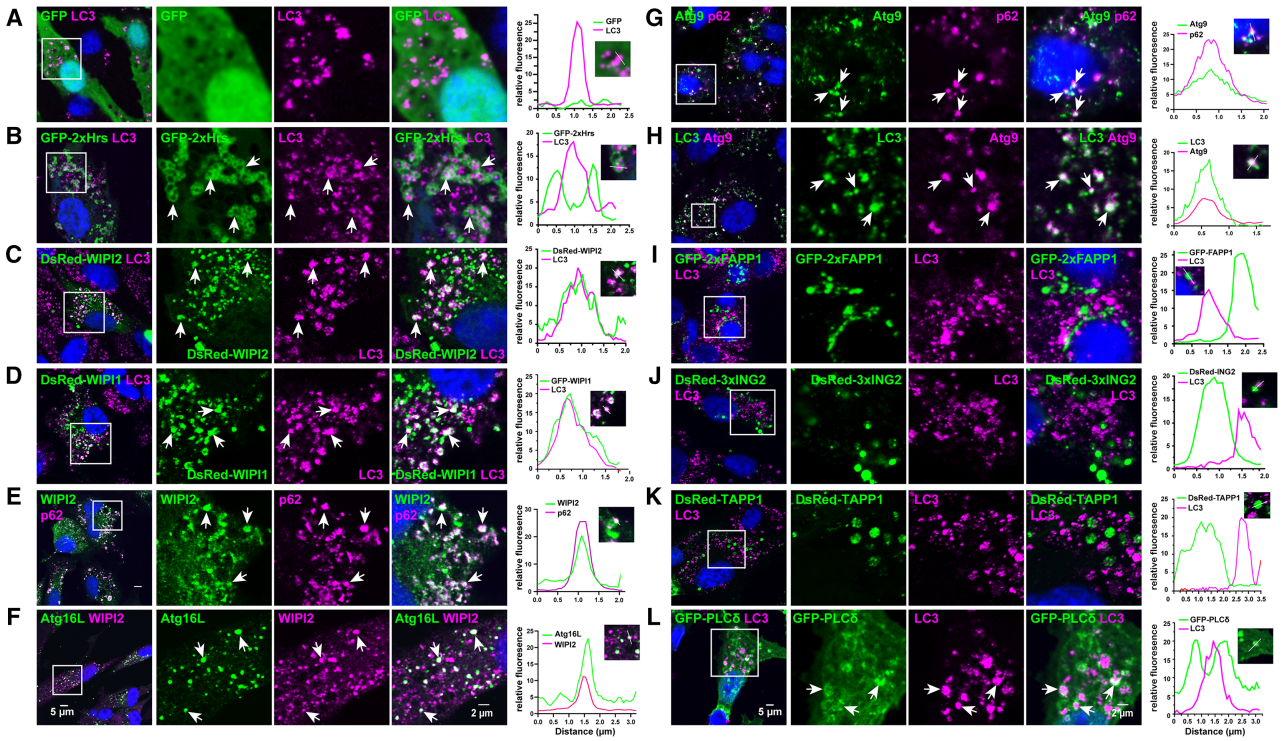

Figure 2. Identification and phosphoinositide contents of autophagy-associated membrane aggregates in chloroquine-treated cultured RPE cells

(A–L) In cultured RPE cells treated with 25 μg/mL chloroquine overnight, autophagy marker LC3 accumulated (A–D and H) and co-localized with WIPI2 (C), WIPI1 (D), and Atg9 (H). In these cells p62 and Atg16L co-localized with WIPI2 (E–F), and Atg9 co-localized with p62 (G). PI(3)P was observed in membranes surrounding, but not truly co-localized with, LC3 puncta (B). Probes for PI(4)P (EGFP-FAPP1, (I)), PI(5)P (DsRed-3xING2, (J)), and PI(3,4)P2 (DsRed-TAPP1, (K)) did not co-localize with LC3. A probe for PI(4,5)P2 (EGFP-PLCδ, (L)) was partially found in membranes surrounding LC3 puncta. Line profiles of intensity for the indicated puncta (*insets*) are plotted on the *far right*. *Arrows* indicate puncta visible in more than one channel for alignment and comparison in adjacent panels.

were not surrounded by LC3-containing membranes. Thus, Vps34 activity and PI(3)P are dispensable for initiation of phagocytosis but are essential for LC3 recruitment and LC3-associated phagocytosis[33,40,41] in cultured ARPE-19 cells.

PI(3)P localization in RPE cells within the mouse eye

To determine the spatial distribution of PI(3)P-enriched membranes in RPE cells in WT retina, we used two different probes. One was the GFP-2xHrs probe[34] described above, expressed from a plasmid introduced using a previously described[29,42] technique in which plasmids are injected into the space between the photoreceptors and the RPE in neonatal (P0) mice, followed by electroporation with polarity selected to drive the plasmid into RPE cells. In these experiments, a similar construct expressing EGFP without a fusion domain was used as a control probe. Using a plasmid encoding our GFP-2XHrs probe (pCAG-GFP-2xHrs), we obtained transfection of a sparse subset of RPE cells in which the green fluorescence could be readily visualized in RPE from fully developed mice (Figures 4A–4C and 5A). EGFP lacking 2xHrs domains (Figure 4Ai), yielded diffuse cytoplasmic fluorescence, with no puncta, whereas the GFP-2XHrs probe yielded multiple puncta corresponding to membranes enriched for PI(3)P (Figures 4Aii, 4Aiii, 4Bi, 4Biii, 4C, and 5A). As a control for the specificity of this probe, we also used it in mice with RPE-specific deletion of active Vps34 (“ΔRPE”, described in detail below) (Figure 4Aiv). The second method for locating PI(3)P (Figures 4D and 5B) used antibodies specific for the endogenous PI(3)P-binding endosome marker EAA1.[43–45] Both these probes revealed two pools of PI(3)P-enriched membranes (Figures 4A–4D and 5B). One consisted of large (>300 nm to several μm) ring-like or annular structures (Figures 4Bi, 4Biii, 4Biv, and 4D) surrounding unlabeled regions which further analysis (see below) revealed to consist of POS phagosomes (see discussion below). The other was a distinct pool of smaller vesicles, many near the diffraction limit (≤300 nm), likely endosomes. Unlike the PI(3)P-enriched autophagosomes that accumulate in many cell types when autophagic flux is blocked, the small PI(3)P-labeled puncta were not positive for autophagic marker p62 (Figure 5B). The larger “hollow” aggregates were seen more often in eyes collected in the mid-morning than in the mid-afternoon, as expected for phagosomes.

PI(3)P on POS phagosomes in WT RPE

To detect phagosomes, we probed RPE of mice with the 1D4 antibody (Figures 4Bii, 4Biii, 4Biv, and 4C), specific for the C-terminal tail of rhodopsin,[46] or used mice heterozygous for the hRho-GFP knockin,[38,39] described above for the *in vitro* experiments (Figures 4D–4H, 6A, 6B, S2A, and S2B). The results showed that in cells expressing WT Vps34, the “hollow”-appearing

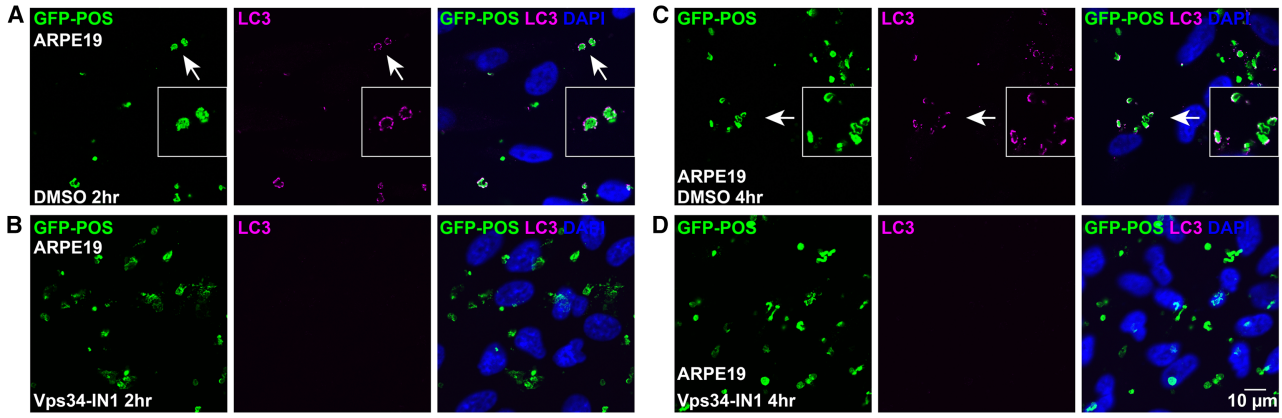

Figure 3. Rod outer segments undergo PI(3)P-dependent LC3-assisted phagocytosis (LAP) in cultured RPE cells

(A–D) POS purified from heterozygous human rhodopsin-GFP knock-in mice were added to ARPE-19 cells for the phagocytosis assay. Cells were pre-treated either with DMSO control (A and C) or Vps34 inhibitor Vps34-IN1 (B and D), incubated with POS for the indicated times, and stained with an antibody directed against LC3. *Insets* show indicated regions at higher magnification. *Arrows* indicate regions magnified in *insets*. Scale as indicated.

compartments were phagosomes containing engulfed POS discs and surrounded by PI(3)P-containing membranes (Figures 4B and 4D). The PI(3)P signal in the large membranes positive for the GFP-2XHrs PI(3)P probe (Figure 4B), or for EEA1 (Figure 4D), a PI(3)P-binding marker of early endosomes,[47,48] could be observed surrounding ingested POS phagosomes (see line profiles Figures 4Biv and 4D1-3). Rather than a single continuous thin membrane enriched in PI(3)P, these appeared as clusters of PI(3)P-positive puncta surrounding the POS, suggesting clusters of endosomes attached to the surface of the phagosomes. The white arrows in Figure 4B indicate a cell not expressing the PI(3)P probe, and containing only a single phagosome, rather than the multiple phagosomes seen in the adjacent transfected cells. This contrast, low numbers of phagosomes in non-transfected cells adjacent to transfected cells with many phagosomes, was observed in multiple fields. This observation suggests that the probe may perturb the PI(3)P-dependent processing of phagosomes, leading to their accumulation. PI(3)P signal was also present in many smaller membranes not containing rhodopsin, likely early endosomes (Figures 4A–4D). Many of the phagosomes were surrounded by membranes positive for the late endosome marker Rab7 (Figure 4D). Some phagosomes were positive for both EEA1 and Rab7 (Figure 4D2), whereas a subset was positive for EEA1 but not Rab7 (Figure 4D1), and yet another was positive for Rab7, but not for EEA1 (Figure 4D3). See line profiles (Figure 4D) for phagosomes labeled 1 for Rab7-negative, EEA1-positive; labeled 2 for Rab7-positive and EEA1-positive; and labeled 3 for Rab7-positive and negative for EEA1.

In radial sections (Figure 4C) it was apparent that the great majority of the small PI(3)P puncta found in WT RPE are located in the basolateral portion of the cells, rather than in the apical processes, which extend to and envelop the distal portions of the POSss. Phagosomes, in contrast, were observed at comparable levels in the basolateral and apical regions (Figures 4C and 4F–4H).

Many, but not all, of the phagosomes were positive for the autophagosome marker LC3 (Figure 4E), whose recruitment to autophagosomes has been reported to depend on the Vps34 complex.[49] While the phagosomes were positive for LC3, typically considered a marker of autophagosomes, they did not stain with antibodies against autophagosome markers WIPI2 (Figure 4F) or Atg9 (Figure 4G) nor for LC3-binding partner, p62 (Figure 4H).

We co-stained with C-terminal-specific antibody 1D4 and an N-terminal-specific rhodopsin antibody, 4D2,[50] and identified three populations of phagosomes (Figures S3A–S3C). These included those that stained only with 1D4, those that stained with only 4D2, and those that stained with both. This result suggests heterogeneity of the phagosomes with respect to proteolytic cleavage of the amino- or carboxy-terminus of rhodopsin.

Effects of knocking out Vps34 activity in the RPE

To serve as a control for these experiments, and to determine the functional role of Vps34 and PI(3)P in RPE cells *in vivo*, we generated mice with mosaic RPE-specific inactivation of Vps34 by starting with mice that were homozygous for a "floxed" (i.e., with *loxP* sites flanking sequence encoding a segment essential for catalysis) allele of Vps34[27] and breeding them with mice that were heterozygous for Cre transgene driven by the RPE-specific VMD2/Best-1 promoter.[51] An advantage of this genotype and the mosaic nature of the knockout is that it allows examining the phenotype of Vps34 knockout cells (expressing Cre; Figures 5, 6, 7, and 8) in the same field as functionally WT cells (not expressing Cre).

Because it had previously been reported that RPE cells expressing Cre in this line have minor defects in nuclear morphology, cell size and tight junction integrity,[52] we characterized the effects of this transgene in the presence of WT Vps34. We examined the retinas of control mice expressing the Best1-Cre transgene, but retaining at least one WT *Vps34* allele, at 4 months post-natal (PN) (Figure 4E), 3 months PN (Figure 5C, middle row; Figure 6A), 2.5 months PN (Figure 5E) and 2 months PN (Figures 8A and S4A–S4C), ages at which the ΔVps34 RPE displays severe phenotypes (massive accumulation of pathological membranes and cell death; discussed in detail below). At all ages, we found that the transgene by itself led to only minor

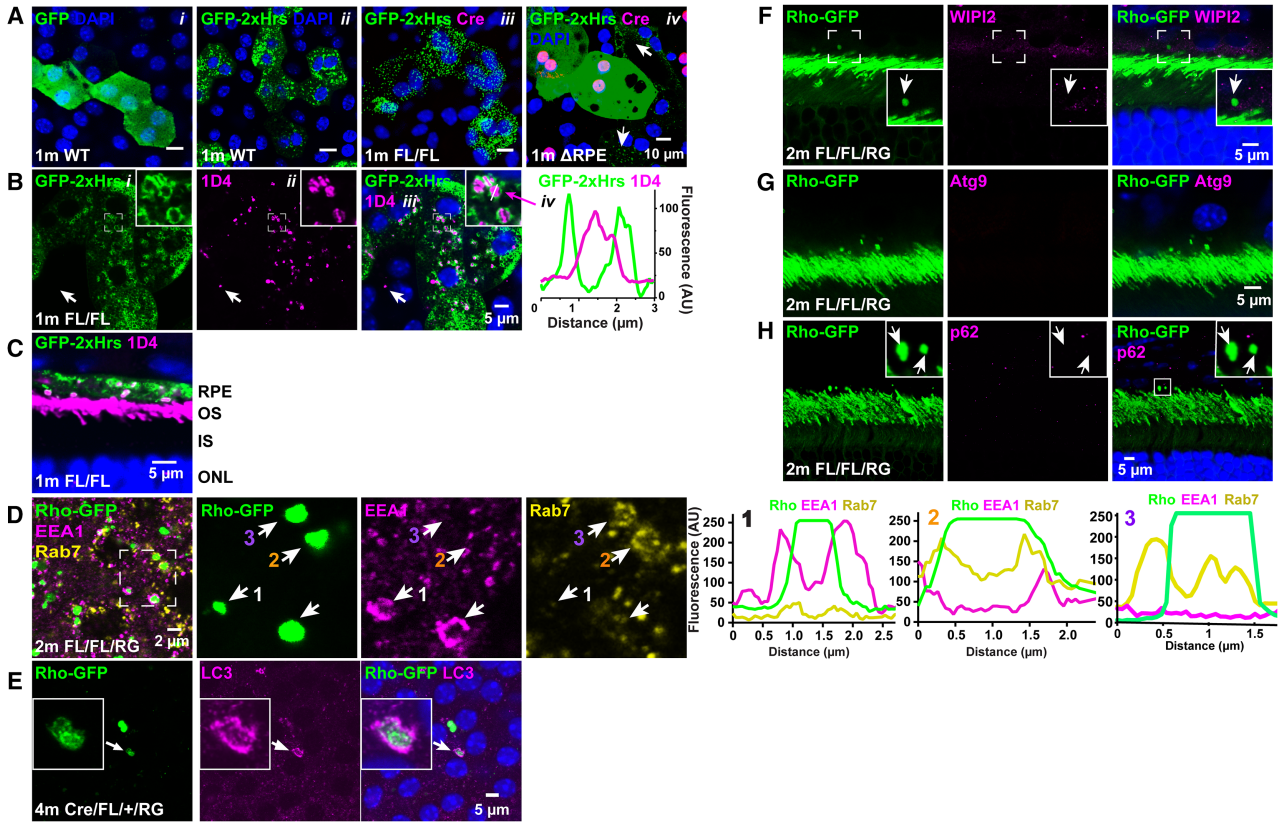

Figure 4. PI(3)P and POS phagosomes in mouse RPE

(A–C) Plasmids expressing GFP (A*i*) or the PI(3)P probe GFP-2xHrs (A*ii*-A*iv*, B*i*-B*iii*) were injected subretinally and electroporated to transfect RPE cells. Flatmount RPE (A and B) and radial eyecup sections (C) revealed multiple PI(3)P puncta in the RPE layer. *Arrows* in A indicate neighboring WT cells with PI(3)P puncta. Staining with anti-rhodopsin antibody 1D4 (B and C) reveals PI(3)P surrounding many 1D4-positive phagosomes. White box in (Bi-Biii) shows area magnified in inset. (Biv) shows line profile of 1D4 and PI(3)P signal across phagosome shown in the inset to (Biii). *White arrow* in (Bi-Biii) shows a single 1D4-positive phagosome in an un-transfected RPE cell lacking GFP-2xHRS signal.

(D–H) Phagosomes in control mice expressing WT Vps34 in RPE and hRho-GFP in rod outer segments. A sparse population of POS phagosomes visualized in flatmounts (D and E) or radial cross-sections (F–H) marked by hRho-GFP can be identified in RPE co-stained with antibodies for other markers. Signals for PI(3)P-binding protein, EEA1 (D), Rab7 (D), or LC3/Atg8 (E) surround POS (line profiles marked **1** and **2** in D).

(F–H) Antibodies for putative PI(3)P-binding protein, WIPI2 (F), and for autophagy markers Atg9 (G) and p62 (H) do not stain POS phagosomes. *Arrows* in panels (D, F, and H) identify corresponding puncta visualized in more than one channel for alignment with other channels in adjacent panels.

defects in cell size and morphology, consistent with the previous report[52] showing minor defects from this transgene in RPE at 3 months PN, and none at one month PN. We also confirmed that no defects were observed in RPE cells homozygous for the floxed Vps34 allele but lacking Cre expression (Figures 5A–5F, 6B, 6C, 7, S2A, S2C, S3A, S3B, and S4A).

As shown in Figures 5A and 4Aiv, cells expressing Cre in mice homozygous for the floxed Vps34 allele (i.e., RPE-specific knockouts) and electroporated with the 2XHrs probe as described above, were lacking PI(3)P-labeled puncta, and showed only a diffuse GFP fluorescence similar to that of EGFP itself, introduced by the same method (Figure 4Ai). Adjacent cells, lacking Cre and therefore expressing the normal complement of WT Vps34, show a normal pattern of PI(3)P puncta (Figure 4Aiv, arrows). Similar results were obtained using, instead of the GFP-2xHrs probe, antibody staining of the endogenous PI(3)P-binding marker of early endosomes, EEA1. EEA1 antibodies stained a large number of puncta in WT RPE cells (Figures 4D and 5B), but none in Vps34 KO cells (Figures 5B and 5F).

In the Vps34 knockout cells, we observed a massive accumulation of autophagy markers, including p62 (Figures 5B, 8A, 8C, 8D, and 8G). Because of the mosaic nature of the knockout, such cells were frequently observed next to WT cells that were completely devoid of detectable p62 signal, and full of EEA1-positive puncta (Figure 5B).

Effects of Vps34 inactivation on RPE cell function and morphology

Typical WT RPE cells are arranged in a hexagonal array, with one to three nuclei per cell (usually two). They stain strongly for the visual cycle protein RPE65 and for markers of the tight junctions between cells, including the protein ZO1 (Figures 5C and 5D) and phalloidin, the stain for filamentous actin (Figure S4A). A frequent observation in the Vps34 KO RPE is empty patches devoid of RPE65 or ZO-1-stained tight junctions over an area the size of

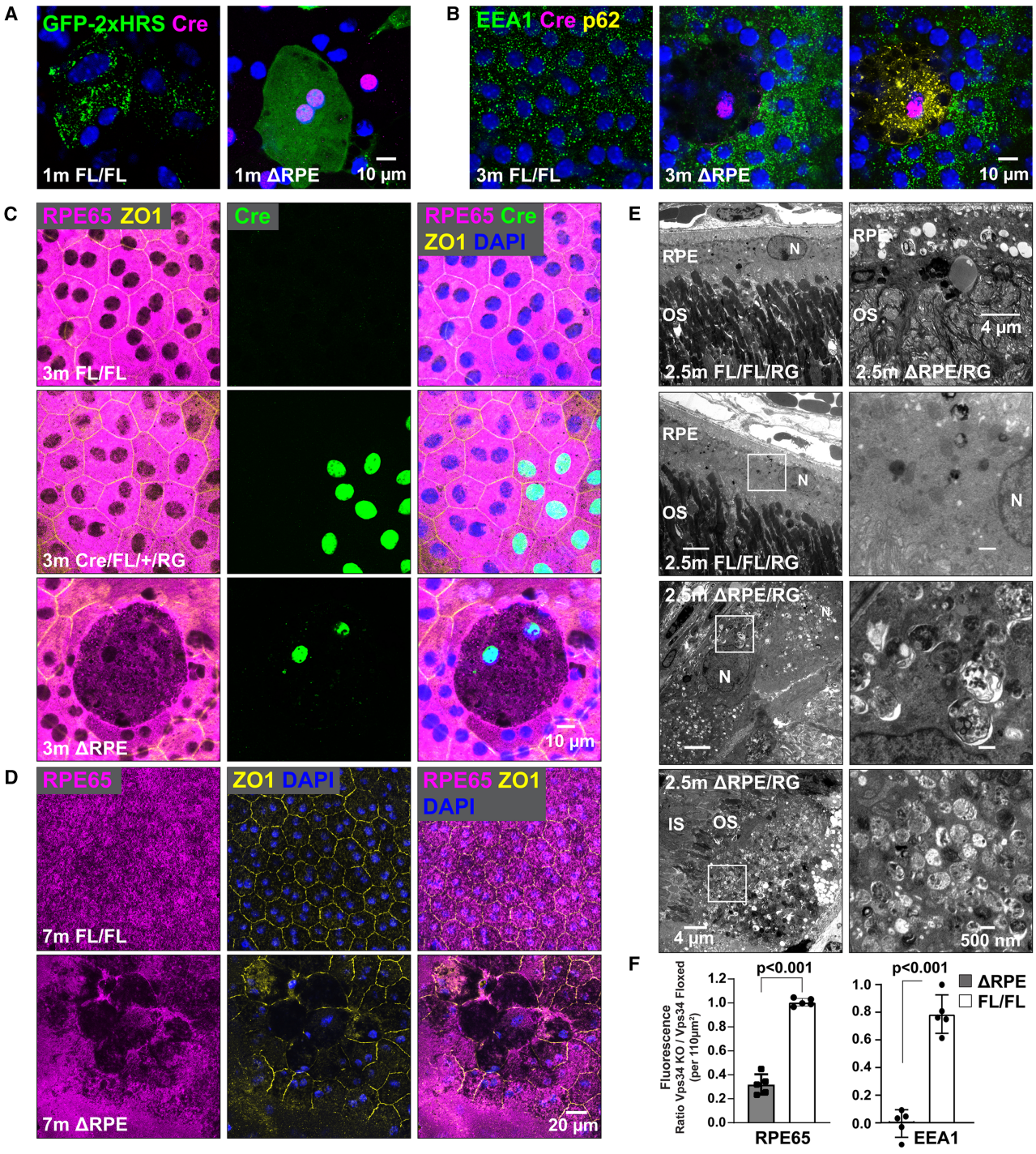

Figure 5. Inactivation of Vps34 in RPE eliminates PI(3)P puncta and leads to cell death and accumulation of aberrant membranes

(A) At 1 month after birth, RPE of mice homozygous for the floxed allele of Vps34 (FL/FL) but not expressing Cre, show WT-like pattern of PI(3)P probe following electroporation of the GFP-2xHrs construct (**left**), but only a diffuse pattern of GFP-2xHRS signal in RPE cells lacking active Vps34 in ΔRPE mice (right).

(B) RPE-specific knockout of Vps34 (ΔRPE) leads to loss of EEA1 puncta and appearance of many aggregates positive for autophagosome marker p62 in Cre-positive cells (middle and right).

(C) At 3 months post-natal, control RPE cells (FL/FL, top row) viewed in flat-mount appear healthy with uniform staining for RPE65, and with intact tight junctions stained for ZO1. Control cells expressing the Best1Cre transgene and one human rhodopsin-GFP but with one WT Vps34 allele (Cre/Fl/+/RG, second row) appeared similarly healthy. In Vps34 KO areas of RPE (ΔRPE, third row), some cells died (missing nuclei), and both tight-junctions (ZO1) and RPE65 staining are lost.

(legend continued on next page)

several normal RPE cells with, at most, one or two surviving nuclei (Figures 5A–5D). When tested, those nuclei were positive for expression of the Cre transgene (Figures 5 and 6). These regions were consistently filled with vesicles and membrane aggregates (Figure 5) positive for autophagy markers such as p62 (Figures 5B, 8C–8E, and 8G), LC3 (Figures 7F, 8A, 8C, and 8F), ATG9 (Figure 8D) and ubiquitin (Figure 8E); see discussion of autophagy-related membranes below.

Electron microscopy of membrane aggregates

We used transmission electron microscopy (TEM) of fixed and stained ultrathin sections to examine the ultrastructure of intracellular membranes in WT and Vps34-functional KO cells (Figures 5E, 6C, and 8B). We observed many structures with multiple layers of membranes that were not observed in mice unless they were homozygous for the *Vps34* floxed allele and expressing Cre in the RPE. Some, but not all, of these structures (magenta arrows in Figure 6C, *red arrows* in Figure 8B) contained what appeared to be stacks of POS discs, representing "stalled" phagosomes, i.e., membranes that had engulfed disc stacks but had not transported them to lysosomes for digestion. Other membranes did not display disc-stack-like morphology, but resembled the multilayered aggregates interpreted as "stalled" autophagy-related membranes in other cells with KO of Vps34 function.[27–32] Many of them resemble in size and appearance objects described as "degradative autophagic vacuoles" (see Figure 3 in Klionsky et al;[53]). These aberrant structures were not observed in WT RPE or in mice homozygous for the floxed Vps34 allele but not expressing Cre, nor in mice with the Best1-Cre transgene but having at least one WT Vps34 allele.

RPE cell death and effects on adjacent photoreceptors

The presence of dying or dead RPE cells observed in flat mount images could be seen in radial sections to have severe deleterious consequences for the adjacent photoreceptors (Figures 5E, 6B, S2B, and S4B). Photoreceptors in the vicinity of Cre-expressing Vps34 KO RPE cells suffered disruption of the structures of the outer segments, including dramatic shortening (Figures 5E, 6B, and S4B).

Accumulation of undigested phagosomes in Vps34 KO RPE

There was a massive accumulation of undigested POS phagosomes in the Vps34 knockout RPE cells, identified either by staining with 1D4, or by using mice bearing a single copy of the hRho-GFP knockin (Figures 6A, 6B, 7, and S2). Unlike control RPE with WT Vps34 (Figures 7A, 7C, 7E, and 7G; *arrows* in A, C, E indicate phagosomes), the phagosomes in Vps34 KO cells were not positive for EEA1 (Figure 7B) nor for LC3 (Figure 7F). They also did not colocalize with the lysosomal marker LAMP2 (Figure 7H) nor with Rab7 (Figure 7D). While there were large numbers of LC3-positive membranes (likely autophagy-related membranes) in the Vps34 KO RPE cells, none of these coincided with the phagosomes containing hRho-GFP (Figure 7E). In TEM images, undigested phagosomes could be recognized by stacks of discs within them (magenta arrows in Figure 6C, *red arrows* in Figure 8B).

Accumulation of autophagy markers in Vps34 KO RPE

As in other cell types with Vps34 deficiencies, there was a massive accumulation of membrane aggregates containing autophagy markers,[53] Atg9, LC3, p62 and ubiquitin (Figures 5B, 7F, 8C–8G, and S3B). The density of p62-positive patches across the entire RPE increased with age, increasing from almost 20 mm^{-2} at 3 months after birth to about 50 mm^{-2} at 10 months postnatal (Figure 8G). A separate set of puncta was positive for lysosomal markers LAMP1 or LAMP2, which did not overlap with the autophagy markers (Figures 7H and 8F). As noted above, TEM images revealed massive accumulation of debris- and membrane-filled vacuoles, that likely correspond to the puncta containing markers of early stages of autophagy (Figures 5E, 6C, 8B). One possible explanation for the accumulation of autophagy-related membranes in the absence of Vps34 catalytic activity is the presence of extremely low levels of PI(3)P in initiation membranes, conceivably derived from a Class II PI-3-kinase or traces of remaining WT Vps34, that are sufficient to recruit PI(3)P-dependent complexes to these membranes in RPE cells. Such a scenario seems unlikely given the inability of Class II PI-3 kinase to substitute for Vps34 in autophagy completion in rod cells, or to substitute for Vps34 in LC3-assisted phagocytosis in RPE. Moreover, in the case of phagosome processing in *Caenorhabditis elegans*, in which Class II PI-3 kinase clearly plays an important role, the levels of PI(3)P produced are readily visible using a 2X-FYVE domain probe similar to the one used here, but of ~10-fold lower affinity.[54–57]

It was previously reported[36] that an alternative probe, containing 4 copies of the Hrs FYVE domain (GFP-4XHrs) could reveal a 35% pool of PI(3)P not detectable by the GFP-2xHrs probe and attributed to the activity of Class II PI(3)-kinase. We prepared and tested this probe extensively (Figures S1A–S1D), as well as a 3X probe, and found that in RPE cells, both fail to detect a persistent pool of PI(3)P when Vps34 is inhibited by Vps34-IN1, a compound that specifically inhibits class III PI3 kinase but not class I or II PI3 kinase.[58] These results, in addition to our previous results in isolated rod cells,[29] demonstrating unequivocal loss of >90% of PI(3)P in the rod-specific Vps34 KO, and the complete loss of LC3 recruitment to phagosomes observed in mouse RPE in the present experiments, along with massive accumulation of undigested debris-filled vesicles, render substantial compensation by Class II PI(3)-kinase highly unlikely.

LC3-independent stimulation of lysosome biogenesis

It was reported recently[59] that phagosome-associated LC3 plays a key role in stimulating lysosome biogenesis by way of transcriptional regulation. However, in Vps34 KO RPE, there is no phagosome-associated LC3, yet there is massive

(D) Larger areas of cell death marked by loss of tight junctions and RPE65 expression are seen at 7 months post-natal.
(E) Transmission electron microscopy (TEM) reveals massive accumulation of aberrant membrane aggregates in Vps34 KO RPE. RPE samples came from mice with the genotypes shown, and all were heterozygous for the hRho-GFP allele.
(F) Quantification of loss of RPE65 signal in Vps34 KO RPE at 3 months post-natal; n = 5 mice.

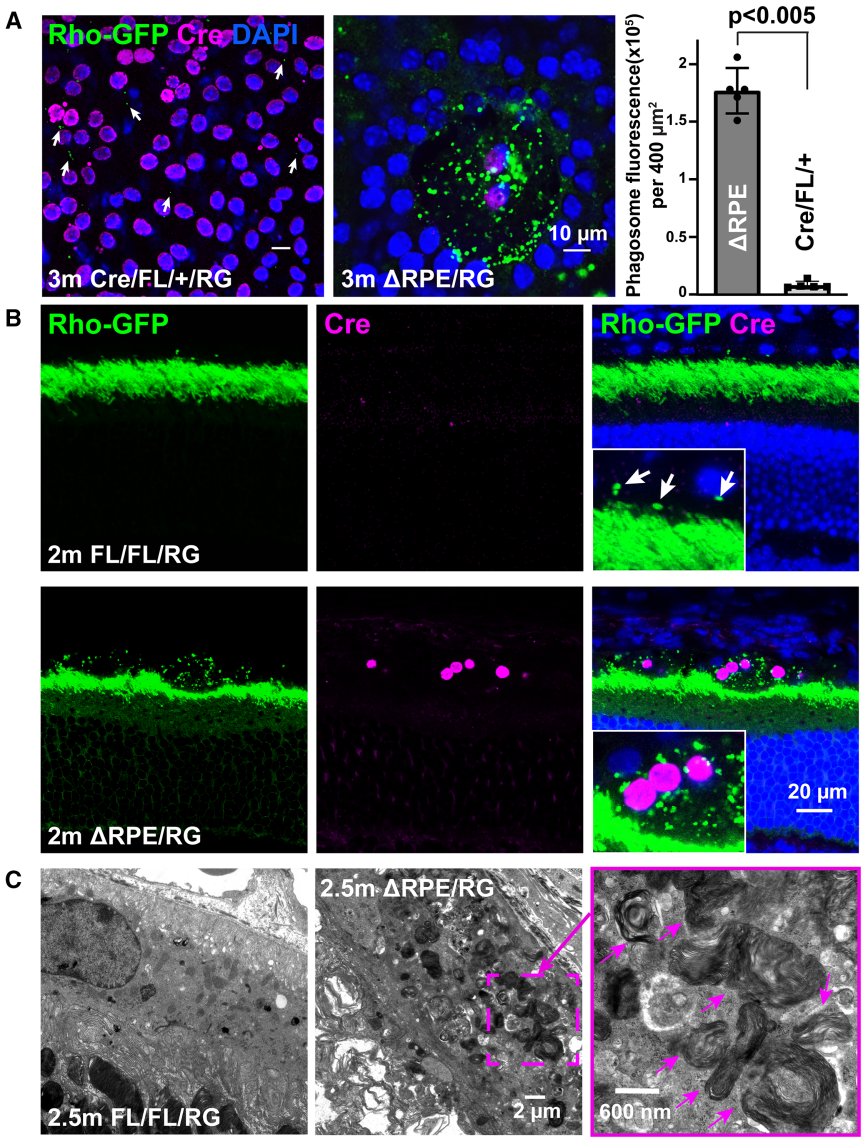

Figure 6. Accumulation of immature phagosomes in Vps34 KO RPE

(A) Flat mount images of RPE from hRho-GFP mice, showing small numbers of small POS phagosomes in control mice, (Cre/FL/+/RG, *arrows*, *left*) but massive accumulation of POS phagosomes in Vps34 KO cells (ΔRPE/RG, *right*) that express Cre. Bar graph in A shows quantification of phagosomes in KO vs. Vps34-expressing fields (*far right*, *n=5* mice).

(B) Radial cross-sections, likewise, show small numbers of phagosomes (*white arrows* in high-magnification *inset* of (B) in control RPE (*upper panels*, FL/FL/RG), but massive phagosome accumulation in Vps34 KO regions with Cre-expressing nuclei (*lower panels* of (B)). Note the thinning of the underlying outer segment layer marked by continuous EGFP fluorescence in KO regions.

(C) TEM shows accumulation of phagosomes with undigested stacks of discs in KO RPE (*middle* and *right* panels, *magenta arrows*), but not in control RPE (*left* panel).

upregulation of lysosomes, as indicated by accumulation of large structures labeled by LAMP1 and LAMP2 (Figures 7H and 8F), indicating that LC3-independent mechanisms for stimulation of lysosome biogenesis are also operative in phagocytosis by RPE cells.

DISCUSSION

Several conclusions can be drawn from these results. One is the absolute requirement for Vps34 catalytic activity and PI(3)P in order to recruit LC3 to phagosomes. This result is in contrast to the observation here in RPE as in multiple other cell types,[27–32,36] that LC3 can be recruited to nascent membranes containing autophagy markers in the absence of Vps34-derived PI(3)P, pointing to substantial differences in the mechanisms available for LC3 recruitment between autophagy and phagocytosis in this cell type. Another interesting observation is that neither PI(3)P nor LC3 recruitment is required for the engulfment of POS by RPE cells in the first stages of phagocytosis. Both by fluorescence and TEM, we observe unequivocal evidence for fully engulfed POS disc stacks within RPE cells lacking Vps34 catalytic activity or any PI(3)P-containing membranes. This result is consistent with results from other phagocytic cells, including macrophages,[3,6] in which it has been found that Class I PI-3 kinase activity and synthesis of PI(3,4,5)P_3 is a necessary step and that the phagocytic cup is enriched in PI(4,5)P_2, rather than PI(3)P, prior to completion of the phagosome membrane. Because of the multiple unique features of RPE phagocytosis[13,14,60–62] it was not previously clear whether the roles of phosphoinositides in RPE mirrored those in macrophages.

Yet another important conclusion is that LAP cannot be accurately described as "non-canonical autophagy", a term that continues to be widely used despite evidence for LAP and autophagy being distinct and competing pathways.[63] Far from being a form of autophagy, LAP is actually antagonistic with autophagy. Previous studies by us and others have shown that phagocytosis in RPE activates mTORC1[63–65] essentially halting autophagy, whereas inhibition of mTOR by rapamycin or starvation has been shown in many cell types to upregulate autophagy dramatically. Phagosomes absolutely require PI(3)P for LC3 recruitment, whereas in RPE cells, as in other cell types[27–32] autophagosomes can recruit LC3 and convert LC3-I to LC3-II by lipidation in the absence of PI(3)P. Apart from PI(3)P and LC3, other characteristic markers of autophagosomes, including p62, Atg9, Atg16L, ubiquitin and WIPI2 are not associated with phagosomes in RPE (Figure S4).

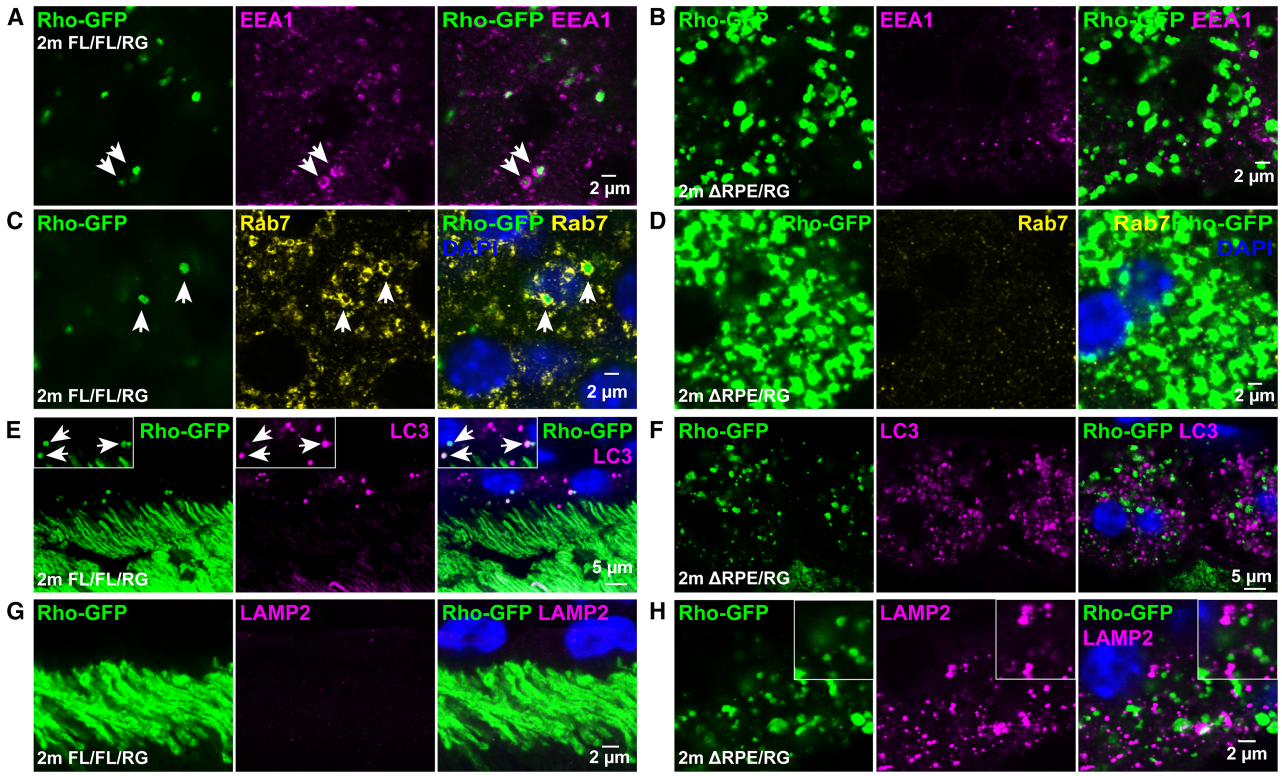

Figure 7. Distinct patterns of markers for endosomes, phagosomes and autophagosomes reveal distinct functions of Vps34

(A–D), flat mounts; (E–H), radial cross-sections. (A) Early endosome marker EEA1 labels multiple small puncta, presumably endosomes, as well as the outside of hRho-GFP labeled phagosomes (*white arrows in* A, C, and E). (B) In Vps34 KO RPE, many hRho-GFP labeled phagosomes accumulate, but they show no overlap with EEA1-labeled structures (likely endosomes). Likewise, Rab7 marks the outside of phagosomes in control RPE (C), but not the large phagosome aggregates in Vps34 KO RPE (D). (E), LC3 is recruited to phagosomes in control RPE, whereas (F), phagosomes in Vps34 KO RPE do not co-stain with LC3 antibodies that stain large numbers of autophagy-related membrane aggregates. Under conditions (G) in which LAMP2-labeled lysosomes are virtually undetectable in control RPE, large numbers of enlarged lysosomes accumulate in VPS34 KO RPE, (H), but show no overlap with Rho-GFP-labeled phagosomes.

Our results also add to our understanding of the sequence of events during POS phagocytosis. The processes of POS engulfment and internalization precede recruitment of Vps34, synthesis of PI(3)P and recruitment of LC3, and do not depend on them. Also, lysosome upregulation does not depend on LC3 recruitment. Subsequent steps of phagosome maturation and processing, however, including trafficking along microtubules, fusion with endosomes or lysosomes, and ultimate degradation, cannot proceed without active Vps34 and PI(3)P.

Finally, the results here confirm observations in other cell types[27–32] that Vps34 is essential for a normal full cycle of autophagy initiation and completion, but not for formation of double-layered and multilayered membranes containing debris, for recruitment of LC3 to non-phagosomal membranes, for formation of LC3-II, or for recruitment of Atg9, p62, and ubiquitinated cargo. Thus, structures bearing hallmarks of autophagy accumulate, but normal autophagy does not proceed.

We are unable to rule out the presence of trace levels of active Vps34 remaining from the pool present prior to gene inactivation in KO cells or undetectably low levels of PI(3)P due to Class II PI-3-kinases. However, the complete failure of LC3 recruitment to phagosomes argues against that scenario, as does the continued accumulation of p62-labeled aggregates (Figure 8) over many months, as well as the rapid loss (minutes) in cultured cells of PI(3)P upon addition of a Vps34 inhibitor (Figure S1).

A remaining mystery is the mechanism(s) by which these autophagy-related membrane aggregates form and recruit autophagy proteins in the absence of Vps34 catalytic activity. It is interesting in this regard to note that somewhat different results were obtained in mouse cells prepared with an alternative knockout construct that leads to the absence of structural Vps34 protein, in contrast to the extensively studied construct used here which yields a structurally intact protein lacking catalytic activity. In the full-knockout case, rather than a massive accumulation of membrane aggregates containing autophagy markers, a reduction in autophagosomes induced by serum starvation was observed.[66] Thus, there may be a structural role for Vps34 in steps dependent on Complex I in addition to its established catalytic role.

Limitations of the study

Firm conclusions are necessarily limited by the available tools. These limitations include lack of definitive evidence that membrane aggregates identified by electron microscopy are identical to those identified by staining with antibodies to autophagy markers. Similarly, identification of membranes by staining with

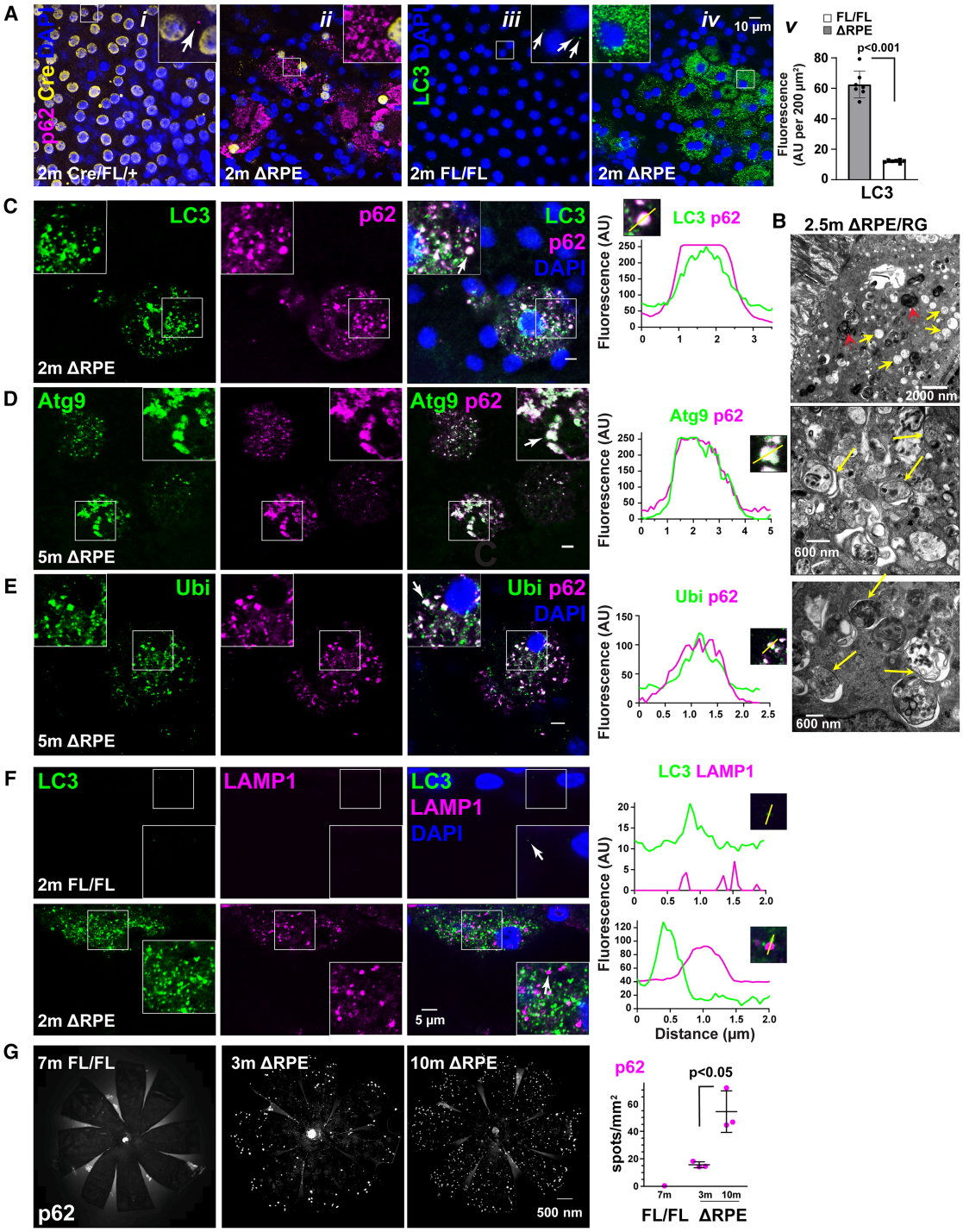

Figure 8. Aggregates positive for autophagy markers accumulate in Vps34 KO RPE

(A) Large numbers of puncta containing p62 (*ii*) and LC3 (*iv*) accumulate in RPE cells lacking Vps34, but neither heterozygous Vps34 KO (*i*) nor homozygosity for the floxed Vps34 allele (*iii*) is sufficient to induce their accumulation. *Arrows* in (Ai) and (Aiii) denote rare p62 or LC3 puncta in cells with functional Vps34. (*v*) Quantification of LC3 signal in RPE cells with (open bar) and without (grey-filled bar) Vps34, $n = 5$ mice.

(B) TEM of Vps34 KO RPE, showing accumulation of large debris-containing vacuoles and multi-layered membrane aggregates. Examples of vacuoles >500 nm in width with visible double membranes are indicated by *yellow arrows*; phagosomes containing undigested discs are indicated by *red arrows*.

(C–E) Co-localization of autophagy markers. Line profiles in far-right panels are from puncta indicated by white arrows in *insets*. p62 co-localizes with LC3 (C), Atg9 (D) and ubiquitin (E) in Vps34 KO RPE.

(legend continued on next page)

one or two antibodies may point strongly to their identities, but cannot be unequivocal. Limitations also include lack of certainty with respect to the progression of the phenotype with time and its precise molecular mechanisms, given the mosaic and time-dependent nature of the conditional knockout.

RESOURCE AVAILABILITY

Lead contact

Requests for further information and resources should be directed to and will be fulfilled by the lead contact, Theodore G. Wensel (twensel@bcm.edu).

Materials availability

Mouse lines, cell lines and antibodies were obtained from indicated commercial sources or academic laboratories and are available from them by purchase or request.

Data and code availability

- Raw data are available upon request to the lead contact. This study did not report any new DNA sequence data or report any new code.
- Any additional information required to reanalyze the data reported in this paper is available from the lead contact upon request.

ACKNOWLEDGMENTS

We acknowledge contributions from the Baylor College of Medicine Genetically Engineered Rodent Core P30 CA125123, and the Vision Science Core (P30-EY002520). This work was supported by National Institutes of Health grants R01-EY031949 and EY026545 to T.G.W. and R01-NS129847 to Zheng Zhou, by Welch Foundation Grant Q0035 to T.G.W., and by Natural Sciences and Engineering Research Council of Canada Discovery Grant (RGPIN-2022-02982) to M.A.A.

AUTHOR CONTRIBUTIONS

F.H. designed experiments, carried out experiments, analyzed data, and worked on writing and revising the manuscript. R.M.N. prepared samples for electron microscopy and collected TEM data. M.A.A. designed and carried out experiments, analyzed data, and edited the manuscript. T.G.W. acquired funding, supervised the project, helped design experiments and analyze data, and contributed to writing and editing the manuscript.

DECLARATION OF INTERESTS

The authors declare no competing interests.

STAR★METHODS

Detailed methods are provided in the online version of this paper and include the following:

SUPPLEMENTAL INFORMATION

Supplemental information can be found online at https://doi.org/10.1016/j.isci.2025.112371.

Received: July 24, 2024
Revised: November 17, 2024
Accepted: April 3, 2025
Published: April 8, 2025

REFERENCES

1. Levine, B., and Klionsky, D.J. (2004). Development by self-digestion: molecular mechanisms and biological functions of autophagy. Dev. Cell *6*, 463–477. https://doi.org/10.1016/s1534-5807(04)00099-1.
2. Simonsen, A., and Tooze, S.A. (2009). Coordination of membrane events during autophagy by multiple class III PI3-kinase complexes. J. Cell Biol. *186*, 773–782. https://doi.org/10.1083/jcb.200907014.
3. Lindmo, K., and Stenmark, H. (2006). Regulation of membrane traffic by phosphoinositide 3-kinases. J. Cell Sci. *119*, 605–614. https://doi.org/10.1242/jcs.02855.
4. Wurmser, A.E., and Emr, S.D. (1998). Phosphoinositide signaling and turnover: Ptdlns(3)P, a regulator of membrane traffic, is transported to the vacuole and degraded by a process that requires lumenal vacuolar hydrolase activities. EMBO J. *17*, 4930–4942. https://doi.org/10.1093/emboj/17.17.4930.
5. Zeng, X., Overmeyer, J.H., and Maltese, W.A. (2006). Functional specificity of the mammalian Beclin-Vps34 PI 3-kinase complex in macroautophagy versus endocytosis and lysosomal enzyme trafficking. J. Cell Sci. *119*, 259–270. https://doi.org/10.1242/jcs.02735.
6. Vieira, O.V., Botelho, R.J., Rameh, L., Brachmann, S.M., Matsuo, T., Davidson, H.W., Schreiber, A., Backer, J.M., Cantley, L.C., and Grinstein, S. (2001). Distinct roles of class I and class III phosphatidylinositol 3-kinases in phagosome formation and maturation. J. Cell Biol. *155*, 19–25. https://doi.org/10.1083/jcb.200107069.
7. Dong, X.-P., Shen, D., Wang, X., Dawson, T., Li, X., Zhang, Q., Cheng, X., Zhang, Y., Weisman, L.S., Delling, M., and Xu, H. (2010). PI(3,5)P(2) controls membrane trafficking by direct activation of mucolipin Ca(2+) release channels in the endolysosome. Nat. Commun. *1*, 38. https://doi.org/10.1038/ncomms1037.
8. Ferguson, C.J., Lenk, G.M., and Meisler, M.H. (2009). Defective autophagy in neurons and astrocytes from mice deficient in PI(3,5)P2. Hum. Mol. Genet. *18*, 4868–4878. https://doi.org/10.1093/hmg/ddp460.
9. Jin, N., Lang, M.J., and Weisman, L.S. (2016). Phosphatidylinositol 3,5-bisphosphate: regulation of cellular events in space and time. Biochem. Soc. Trans. *44*, 177–184. https://doi.org/10.1042/bst20150174.

(F) Large aggregates containing lysosomal marker LAMP1 accumulate, but do not co-localize with aggregates of autophagy markers labeled by LC3, in Vps34 KO RPE cells (lower row) but not in floxed control cells (upper row). *Arrows* in (C–E) indicate puncta selected for the line profiles plotted to the right of the images. The number of cells filled with autophagy-related aggregates marked by p62 increases with age (G). Low-magnification images were digitally stitched to cover the entire eyecup. Increase in total eyecup p62 signal with age is quantified in plot on far right (n = 3 mice).

10. Kiser, P.D., and Palczewski, K. (2021). Pathways and disease-causing alterations in visual chromophore production for vertebrate vision. J. Biol. Chem. *296*, 100072. https://doi.org/10.1074/jbc.REV120.014405.

11. Saari, J.C. (2016). Vitamin A and Vision. Subcell. Biochem. *81*, 231–259. https://doi.org/10.1007/978-94-024-0945-1_9.

12. Wright, C.B., Redmond, T.M., and Nickerson, J.M. (2015). A History of the Classical Visual Cycle. Prog. Mol. Biol. Transl. Sci. *134*, 433–448. https://doi.org/10.1016/bs.pmbts.2015.06.009.

13. Kevany, B.M., and Palczewski, K. (2010). Phagocytosis of retinal rod and cone photoreceptors. Physiology *25*, 8–15. https://doi.org/10.1152/physiol.00038.2009.

14. LaVail, M.M. (1983). Outer segment disc shedding and phagocytosis in the outer retina. Trans. Ophthalmol. Soc. UK *103*, 397–404.

15. LaVail, M.M. (1976). Rod outer segment disk shedding in rat retina: relationship to cyclic lighting. Science *194*, 1071–1074. https://doi.org/10.1126/science.982063.

16. Young, R.W., and Bok, D. (1969). Participation of the retinal pigment epithelium in the rod outer segment renewal process. J. Cell Biol. *42*, 392–403.

17. Kaur, G., Tan, L.X., Rathnasamy, G., La Cunza, N., Germer, C.J., Toops, K. A., Fernandes, M., Blenkinsop, T.A., and Lakkaraju, A. (2018). Aberrant early endosome biogenesis mediates complement activation in the retinal pigment epithelium in models of macular degeneration. Proc. Natl. Acad. Sci. USA *115*, 9014–9019. https://doi.org/10.1073/pnas.1805039115.

18. Shang, P., Stepicheva, N., Teel, K., McCauley, A., Fitting, C.S., Hose, S., Grebe, R., Yazdankhah, M., Ghosh, S., Liu, H., et al. (2021). βA3/A1-crystallin regulates apical polarity and EGFR endocytosis in retinal pigmented epithelial cells. Commun. Biol. *4*, 850. https://doi.org/10.1038/s42003-021-02386-6.

19. Hollyfield, J.G., Varner, H.H., Rayborn, M.E., Liou, G.I., and Bridges, C.D. (1985). Endocytosis and degradation of interstitial retinol-binding protein: differential capabilities of cells that border the interphotoreceptor matrix. J. Cell Biol. *100*, 1676–1681. https://doi.org/10.1083/jcb.100.5.1676.

20. Intartaglia, D., Giamundo, G., and Conte, I. (2022). Autophagy in the retinal pigment epithelium: a new vision and future challenges. FEBS J. *289*, 7199–7212. https://doi.org/10.1111/febs.16018.

21. Kaarniranta, K., Blasiak, J., Liton, P., Boulton, M., Klionsky, D.J., and Sinha, D. (2023). Autophagy in age-related macular degeneration. Autophagy *19*, 388–400. https://doi.org/10.1080/15548627.2022.2069437.

22. Kononenko, N.L., Claßen, G.A., Kuijpers, M., Puchkov, D., Maritzen, T., Tempes, A., Malik, A.R., Skalecka, A., Bera, S., Jaworski, J., and Haucke, V. (2017). Retrograde transport of TrkB-containing autophagosomes via the adaptor AP-2 mediates neuronal complexity and prevents neurodegeneration. Nat. Commun. *8*, 14819. https://doi.org/10.1038/ncomms14819.

23. Kimura, N., Kumamoto, T., Kawamura, Y., Himeno, T., Nakamura, K.I., Ueyama, H., and Arakawa, R. (2007). Expression of autophagy-associated genes in skeletal muscle: an experimental model of chloroquine-induced myopathy. Pathobiology *74*, 169–176. https://doi.org/10.1159/000103376.

24. Noda, T., Fujita, N., and Yoshimori, T. (2009). The late stages of autophagy: how does the end begin? Cell Death Differ. *16*, 984–990. https://doi.org/10.1038/cdd.2009.54.

25. Ohashi, Y. (2021). Activation Mechanisms of the VPS34 Complexes. Cells *10*, 3124. https://doi.org/10.3390/cells10113124.

26. Chang, Y.Y., Juhász, G., Goraksha-Hicks, P., Arsham, A.M., Mallin, D.R., Muller, L.K., and Neufeld, T.P. (2009). Nutrient-dependent regulation of autophagy through the target of rapamycin pathway. Biochem. Soc. Trans. *37*, 232–236. https://doi.org/10.1042/bst0370232.

27. Zhou, X., Wang, L., Hasegawa, H., Amin, P., Han, B.X., Kaneko, S., He, Y., and Wang, F. (2010). Deletion of PIK3C3/Vps34 in sensory neurons causes rapid neurodegeneration by disrupting the endosomal but not the autophagic pathway. Proc. Natl. Acad. Sci. USA *107*, 9424–9429. https://doi.org/10.1073/pnas.0914725107.

28. He, F., Nichols, R.M., Kailasam, L., Wensel, T.G., and Agosto, M.A. (2019). Critical Role for Phosphatidylinositol-3 Kinase Vps34/PIK3C3 in ON-Bipolar Cells. Investig. Ophthalmol. Vis. Sci. *60*, 2861–2874. https://doi.org/10.1167/iovs.19-26586.

29. He, F., Agosto, M.A., Anastassov, I.A., Tse, D.Y., Wu, S.M., and Wensel, T. G. (2016). Phosphatidylinositol-3-phosphate is light-regulated and essential for survival in retinal rods. Sci. Rep. *6*, 26978. https://doi.org/10.1038/srep26978.

30. Jaber, N., Dou, Z., Lin, R.Z., Zhang, J., and Zong, W.X. (2012). Mammalian PIK3C3/VPS34: the key to autophagic processing in liver and heart. Autophagy *8*, 707–708. https://doi.org/10.4161/auto.19627.

31. Bechtel, W., Helmstädter, M., Balica, J., Hartleben, B., Schell, C., and Huber, T.B. (2013). The class III phosphatidylinositol 3-kinase PIK3C3/VPS34 regulates endocytosis and autophagosome-autolysosome formation in podocytes. Autophagy *9*, 1097–1099. https://doi.org/10.4161/auto.24634.

32. Reifler, A., Li, X., Archambeau, A.J., McDade, J.R., Sabha, N., Michele, D. E., and Dowling, J.J. (2014). Conditional knockout of pik3c3 causes a murine muscular dystrophy. Am. J. Pathol. *184*, 1819–1830. https://doi.org/10.1016/j.ajpath.2014.02.012.

33. Pena-Martinez, C., Rickman, A.D., and Heckmann, B.L. (2022). Beyond autophagy: LC3-associated phagocytosis and endocytosis. Sci. Adv. *8*, eabn1702. https://doi.org/10.1126/sciadv.abn1702.

34. Gillooly, D.J., Morrow, I.C., Lindsay, M., Gould, R., Bryant, N.J., Gaullier, J. M., Parton, R.G., and Stenmark, H. (2000). Localization of phosphatidylinositol 3-phosphate in yeast and mammalian cells. EMBO J. *19*, 4577–4588. https://doi.org/10.1093/emboj/19.17.4577.

35. Polson, H.E.J., de Lartigue, J., Rigden, D.J., Reedijk, M., Urbé, S., Clague, M.J., and Tooze, S.A. (2010). Mammalian Atg18 (WIPI2) localizes to omegasome-anchored phagophores and positively regulates LC3 lipidation. Autophagy *6*, 506–522. https://doi.org/10.4161/auto.6.4.11863.

36. Devereaux, K., Dall'Armi, C., Alcazar-Roman, A., Ogasawara, Y., Zhou, X., Wang, F., Yamamoto, A., De Camilli, P., and Di Paolo, G. (2013). Regulation of mammalian autophagy by class II and III PI 3-kinases through PI3P synthesis. PLoS One *8*, e76405. https://doi.org/10.1371/journal.pone.0076405.

37. Ho, C.Y., Alghamdi, T.A., and Botelho, R.J. (2012). Phosphatidylinositol-3,5-bisphosphate: no longer the poor PIP2. Traffic *13*, 1–8. https://doi.org/10.1111/j.1600-0854.2011.01246.x.

38. Wensel, T.G., Gross, A.K., Chan, F., Sykoudis, K., and Wilson, J.H. (2005). Rhodopsin-EGFP knock-ins for imaging quantal gene alterations. Vision Res. *45*, 3445–3453. S0042-6989(05)00359-7.

39. Chan, F., Bradley, A., Wensel, T.G., and Wilson, J.H. (2004). Knock-in human rhodopsin-GFP fusions as mouse models for human disease and targets for gene therapy. Proc. Natl. Acad. Sci. USA *101*, 9109–9114.

40. Heckmann, B.L., Boada-Romero, E., Cunha, L.D., Magne, J., and Green, D.R. (2017). LC3-Associated Phagocytosis and Inflammation. J. Mol. Biol. *429*, 3561–3576. https://doi.org/10.1016/j.jmb.2017.08.012.

41. Kim, J.Y., Zhao, H., Martinez, J., Doggett, T.A., Kolesnikov, A.V., Tang, P. H., Ablonczy, Z., Chan, C.C., Zhou, Z., Green, D.R., and Ferguson, T.A. (2013). Noncanonical autophagy promotes the visual cycle. Cell *154*, 365–376. https://doi.org/10.1016/j.cell.2013.06.012.

42. Matsuda, T., and Cepko, C.L. (2004). Electroporation and RNA interference in the rodent retina in vivo and in vitro. Proc. Natl. Acad. Sci. USA *101*, 16–22.

43. Patki, V., Virbasius, J., Lane, W.S., Toh, B.H., Shpetner, H.S., and Corvera, S. (1997). Identification of an early endosomal protein regulated by phosphatidylinositol 3-kinase. Proc. Natl. Acad. Sci. USA *94*, 7326–7330. https://doi.org/10.1073/pnas.94.14.7326.

44. Stenmark, H., Aasland, R., Toh, B.H., and D'Arrigo, A. (1996). Endosomal localization of the autoantigen EEA1 is mediated by a zinc-binding FYVE finger. J. Biol. Chem. *271*, 24048–24054. https://doi.org/10.1074/jbc.271.39.24048.

45. Mu, F.T., Callaghan, J.M., Steele-Mortimer, O., Stenmark, H., Parton, R. G., Campbell, P.L., McCluskey, J., Yeo, J.P., Tock, E.P., and Toh, B.H. (1995). EEA1, an early endosome-associated protein. EEA1 is a conserved alpha-helical peripheral membrane protein flanked by cysteine "fingers" and contains a calmodulin-binding IQ motif. J. Biol. Chem. *270*, 13503–13511. https://doi.org/10.1074/jbc.270.22.13503.

46. Molday, R.S., and MacKenzie, D. (1983). Monoclonal antibodies to rhodopsin: characterization, cross-reactivity, and application as structural probes. Biochemistry *22*, 653–660.

47. Kutateladze, T.G., and Overduin, M. (2001). Structural mechanism of endosome docking by the FYVE domain. Science *291*, 1793–1796.

48. Raiborg, C., Bremnes, B., Mehlum, A., Gillooly, D.J., D'Arrigo, A., Stang, E., and Stenmark, H. (2001). FYVE and coiled-coil domains determine the specific localisation of Hrs to early endosomes. J. Cell Sci. *114*, 2255–2263. https://doi.org/10.1242/jcs.114.12.2255.

49. Yang, Z., and Klionsky, D.J. (2010). Mammalian autophagy: core molecular machinery and signaling regulation. Curr. Opin. Cell Biol. *22*, 124–131. https://doi.org/10.1016/j.ceb.2009.11.014.

50. Laird, D.W., and Molday, R.S. (1988). Evidence against the role of rhodopsin in rod outer segment binding to RPE cells. Investig. Ophthalmol. Vis. Sci. *29*, 419–428.

51. Iacovelli, J., Zhao, C., Wolkow, N., Veldman, P., Gollomp, K., Ojha, P., Lukinova, N., King, A., Feiner, L., Esumi, N., et al. (2011). Generation of Cre transgenic mice with postnatal RPE-specific ocular expression. Investig. Ophthalmol. Vis. Sci. *52*, 1378–1383. https://doi.org/10.1167/iovs.10-6347.

52. He, L., Marioutina, M., Dunaief, J.L., and Marneros, A.G. (2014). Age- and gene-dosage-dependent cre-induced abnormalities in the retinal pigment epithelium. Am. J. Pathol. *184*, 1660–1667. https://doi.org/10.1016/j.ajpath.2014.02.007.

53. Klionsky, D.J., Abdel-Aziz, A.K., Abdelfatah, S., Abdellatif, M., Abdoli, A., Abel, S., Abeliovich, H., Abildgaard, M.H., Abudu, Y.P., Acevedo-Arozena, A., et al. (2021). Guidelines for the use and interpretation of assays for monitoring (4th edition)[1]. Autophagy *17*, 1–382. https://doi.org/10.1080/15548627.2020.1797280.

54. Cheng, S., Wang, K., Zou, W., Miao, R., Huang, Y., Wang, H., and Wang, X. (2015). PtdIns(4,5)P_2 and PtdIns3P coordinate to regulate phagosomal sealing for apoptotic cell clearance. J. Cell Biol. *210*, 485–502. https://doi.org/10.1083/jcb.201501038.

55. Cheng, S., Wu, Y., Lu, Q., Yan, J., Zhang, H., and Wang, X. (2013). Autophagy genes coordinate with the class II PI/PtdIns 3-kinase PIKI-1 to regulate apoptotic cell clearance in C. elegans. Autophagy *9*, 2022–2032. https://doi.org/10.4161/auto.26323.

56. Lu, N., Shen, Q., Mahoney, T.R., Neukomm, L.J., Wang, Y., and Zhou, Z. (2012). Two PI 3-kinases and one PI 3-phosphatase together establish the cyclic waves of phagosomal PtdIns(3)P critical for the degradation of apoptotic cells. PLoS Biol. *10*, e1001245. https://doi.org/10.1371/journal.pbio.1001245.

57. Furutani, M., Tsujita, K., Itoh, T., Ijuin, T., and Takenawa, T. (2006). Application of phosphoinositide-binding domains for the detection and quantification of specific phosphoinositides. Anal. Biochem. *355*, 8–18. https://doi.org/10.1016/j.ab.2006.05.014.

58. Bago, R., Malik, N., Munson, M.J., Prescott, A.R., Davies, P., Sommer, E., Shpiro, N., Ward, R., Cross, D., Ganley, I.G., and Alessi, D.R. (2014). Characterization of VPS34-IN1, a selective inhibitor of Vps34, reveals that the phosphatidylinositol 3-phosphate-binding SGK3 protein kinase is a downstream target of class III phosphoinositide 3-kinase. Biochem. J. *463*, 413–427. https://doi.org/10.1042/BJ20140889.

59. Tan, L.X., Germer, C.J., Thamban, T., La Cunza, N., and Lakkaraju, A. (2023). Optineurin tunes outside-in signaling to regulate lysosome biogenesis and phagocytic clearance in the retina. Curr. Biol. *33*, 3805–3820.e7. https://doi.org/10.1016/j.cub.2023.07.031.

60. Nguyen-Legros, J., and Hicks, D. (2000). Renewal of photoreceptor outer segments and their phagocytosis by the retinal pigment epithelium. Int. Rev. Cytol. *196*, 245–313.

61. Lieffrig, S.A., Gyimesi, G., Mao, Y., and Finnemann, S.C. (2023). Clearance phagocytosis by the retinal pigment epithelial during photoreceptor outer segment renewal: Molecular mechanisms and relation to retinal inflammation. Immunol. Rev. *319*, 81–99. https://doi.org/10.1111/imr.13264.

62. Lakkaraju, A., Umapathy, A., Tan, L.X., Daniele, L., Philp, N.J., Boesze-Battaglia, K., and Williams, D.S. (2020). The cell biology of the retinal pigment epithelium. Prog. Retin. Eye Res. *2020*, 100846. https://doi.org/10.1016/j.preteyeres.2020.100846.

63. Muniz-Feliciano, L., Doggett, T.A., Zhou, Z., and Ferguson, T.A. (2017). RUBCN/rubicon and EGFR regulate lysosomal degradative processes in the retinal pigment epithelium (RPE) of the eye. Autophagy *13*, 2072–2085. https://doi.org/10.1080/15548627.2017.1380124.

64. Go, Y.M., Zhang, J., Fernandes, J., Litwin, C., Chen, R., Wensel, T.G., Jones, D.P., Cai, J., and Chen, Y. (2020). MTOR-initiated metabolic switch and degeneration in the retinal pigment epithelium. FASEB J. *34*, 12502–12520. https://doi.org/10.1096/fj.202000612R.

65. Yu, B., Egbejimi, A., Dharmat, R., Xu, P., Zhao, Z., Long, B., Miao, H., Chen, R., Wensel, T.G., Cai, J., and Chen, Y. (2018). Phagocytosed photoreceptor outer segments activate mTORC1 in the retinal pigment epithelium. Sci. Signal. *11*, eaag3315. https://doi.org/10.1126/scisignal.aag3315.

66. Jaber, N., Dou, Z., Chen, J.S., Catanzaro, J., Jiang, Y.P., Ballou, L.M., Selinger, E., Ouyang, X., Lin, R.Z., Zhang, J., and Zong, W.X. (2012). Class III PI3K Vps34 plays an essential role in autophagy and in heart and liver function. Proc. Natl. Acad. Sci. USA *109*, 2003–2008. https://doi.org/10.1073/pnas.1112848109.

67. Agosto, M.A., Zhang, Z., He, F., Anastassov, I.A., Wright, S.J., McGehee, J., and Wensel, T.G. (2014). Oligomeric state of purified transient receptor potential melastatin-1 (TRPM1), a protein essential for dim light vision. J. Biol. Chem. *289*, 27019–27033. https://doi.org/10.1074/jbc.M114.593780.

68. Gimenez, E., and Montoliu, L. (2001). A simple polymerase chain reaction assay for genotyping the retinal degeneration mutation (Pdeb(rd1)) in FVB/N-derived transgenic mice. Lab. Anim. *35*, 153–156. https://doi.org/10.1258/0023677011911525.

69. Mattapallil, M.J., Wawrousek, E.F., Chan, C.C., Zhao, H., Roychoudhury, J., Ferguson, T.A., and Caspi, R.R. (2012). The Rd8 mutation of the Crb1 gene is present in vendor lines of C57BL/6N mice and embryonic stem cells, and confounds ocular induced mutant phenotypes. Investig. Ophthalmol. Vis. Sci. *53*, 2921–2927. https://doi.org/10.1167/iovs.12-9662.

70. Dowler, S., Currie, R.A., Campbell, D.G., Deak, M., Kular, G., Downes, C.P., and Alessi, D.R. (2000). Identification of pleckstrin-homology-domain-containing proteins with novel phosphoinositide-binding specificities. Biochem. J. *351*, 19–31. https://doi.org/10.1042/0264-6021:3510019.

71. Stauffer, T.P., Ahn, S., and Meyer, T. (1998). Receptor-induced transient reduction in plasma membrane PtdIns(4,5)P2 concentration monitored in living cells. Curr. Biol. *8*, 343–346. https://doi.org/10.1016/s0960-9822(98)70135-6.

72. Pedeux, R., Sengupta, S., Shen, J.C., Demidov, O.N., Saito, S., Onogi, H., Kumamoto, K., Wincovitch, S., Garfield, S.H., McMenamin, M., et al. (2005). ING2 regulates the onset of replicative senescence by induction of p300-dependent p53 acetylation. Mol. Cell Biol. *25*, 6639–6648. https://doi.org/10.1128/MCB.25.15.6639-6648.2005.

73. Itakura, E., and Mizushima, N. (2010). Characterization of autophagosome formation site by a hierarchical analysis of mammalian Atg proteins. Autophagy *6*, 764–776. https://doi.org/10.4161/auto.6.6.12709.

74. Schindelin, J., Arganda-Carreras, I., Frise, E., Kaynig, V., Longair, M., Pietzsch, T., Preibisch, S., Rueden, C., Saalfeld, S., Schmid, B., et al. (2012). Fiji: an open-source platform for biological-image analysis. Nat. Methods *9*, 676–682. https://doi.org/10.1038/nmeth.2019.

75. Wensel, T.G., and Gilliam, J.C. (2015). Three-dimensional architecture of murine rod cilium revealed by cryo-EM. Methods Mol. Biol. *1271*, 267–292. https://doi.org/10.1007/978-1-4939-2330-4_18.

76. Mazzoni, F., Mao, Y., and Finnemann, S.C. (2019). Advanced Analysis of Photoreceptor Outer Segment Phagocytosis by RPE Cells in Culture. Methods Mol. Biol. *1834*, 95–108. https://doi.org/10.1007/978-1-4939-8669-9_7.

77. Agosto, M.A., Anastassov, I.A., Robichaux, M.A., and Wensel, T.G. (2018). A Large Endoplasmic Reticulum-Resident Pool of TRPM1 in Retinal ON-Bipolar Cells. eNeuro *5*. https://doi.org/10.1523/ENEURO.0143-18.2018.

STAR★METHODS

KEY RESOURCES TABLE

REAGENT or RESOURCE	SOURCE	IDENTIFIER
Antibodies		
rabbit anti-Cre	EMD-Millipore	69050
mouse anti-ubiquitin	EMD-Millipore	04-263
rabbit anti-GRP78/BiP	Thermo Fisher	PA1-014A
rabbit anti-TGN46	Thermo Fisher	PA5-23068
Armenian hamster anti-Atg9	Thermo Fisher	MA1-149
rabbit anti ZO-1/TJP1	Thermo Fisher	402200
Alexa Fluor 647 phalloidin	Thermo Fisher	A22287
mouse anti-GM130	BD Biosciences	610822
rabbit anti-Rab5	Cell Signaling	3547, C8B1
rabbit anti-Rab7	Cell Signaling	8558, D12B11
rabbit anti-LC3A/B	Cell Signaling	12741
mouse anti-EEA1	Cell Signaling	48453 E9Q6G,
mouse anti-LC3	Abgent	AM1800a
guinea pig anti-p62	Amer. Research Prod.	03-GP62-C
mouse anti-LAMP2	Abcam	ab25631
rabbit anti-Rab11	Abcam	ab128913
rabbit anti-Atg9	Abcam	PA1-16993
mouse anti-RPE65	Abcam	MA1-16578
mouse anti-LAMP1	Calbiochem	428017
mouse anti-Atg16L	MBL	M150
rabbit anti-Atg16L	MBL	PM040
Donkey secondary antibodies, Alexa dye-conjugated: Anti-rabbit IgG (H + L) Alexa Fluor 488	Thermo	A21206
Anti-mouse IgG (H+L) Alexa Fluor 488	Thermo	A21202
Anti-mouse IgG, Alexa Fluor 647	Thermo	A31571
Anti-rabbit IgG, H+L, Alexa Fluor 555	Thermo	A32794
Anti-mouse IgG Alexa Fluor Plus 555	Thermo	A32773
1D4, mouse monoclonal anti-rhodopsin C-terminus	Prepared in house as described in Agosto et al.[67]	1D4, described in Molday & MacKenzie[46]
4D2	EMD millipore	MABN15
Rabbit anti-LC3	Cell Signaling	12741S
Mouse anti-WIPI2	Abcam	ab105459
Mouse anti-WIPI1	Abcam	ab128901
Rabbit anti-Sec61	EMD Millipore	07-204
Donkey anti-Rabbit IgG (H+L) Alexa Fluor™ 647	Thermo	A315773
Goat anti-Hamster IgG (H+L), Alexa Fluor™ 647,	Thermo	A21451
Goat anti-Mouse IgG1, Alexa Fluor™ 488	Thermo	A21121
Goat anti-Mouse IgG2b, Alexa Fluor™ 555	Thermo	A2247
Nunc™ Lab-Tek™ II Chambered Coverglass	Thermo	155409

(*Continued on next page*)

Continued

REAGENT or RESOURCE	SOURCE	IDENTIFIER
Bacterial and virus strains		
BL21(DE3)pLysS E. coli	(MilliporeSigma, Burlington, MA)	69451-3
Chemicals, peptides, and recombinant proteins		
chloroquine diphosphate	MilliporeSigma	C6628
Lipomaster 3000	Vazyme	TL301-00
Glutaraldehyde	EMS	16020
Osmium tetroxide	Sigma	201030
Vps34IN1	Selleckchem	S7980
ViaFect transfection reagent	Promega	E4981
GIBCO Opti-MEM I reduced serum medium	Fisher Scientific	31985062
OCT	Tissue-Tek	62550
Opti-prep (iodixanol)	Sigma-Aldrich	D1556
DAPI	sigma	D9542
PBS	corning	21-040-CV
Triton-X100	Sigma	93443
DMSO	sigma	D2650
paraformaldehyde	EMS	15710
Vectashield anti-fade reagent	Vector Laboratories	H-1200
Prolong gold mounting medium	Thermo	P36961
Donkey serum	Jackson immune. Research Lab	017-000-121
BSA	Sigma	A9647
Fish gelatin	Sigma	G7765
MFG-E8	R & D Systems	2767-MF-050
Gas6	R & D Systems	885-GSB-050
Sodium cacodylate trihydrate	Sigma	C4945
Glutathione Sepharose High Performance GST-tagged protein purification resin	Cytyiva	17527901
PI(3)P diC16	Echelon	P-3016
DPPC	Echelon	L-1116
DPPS	Echelon	L-3116
DOPE	Echelon	L-2182
SuperSignal™ ELISA Femto Substrate	Thermo	37074
Experimental models: Cell lines		
ARPE-19	ATTC	CRL-2302
Experimental models: Organisms/strains		
C57BL/6J (WT mice)	Jackson Laboratory	C57BL/6J
B6 albino (B6(Cg)-Tyrc-2J/J) (albino mice)	Jackson Laboratory	B6(Cg)-Tyrc-2J/J
Mice with transgene expressing *Cre* under control of *BEST-1* promoter[51]	Jackson Laboratory	C57BL/6-Tg(*BEST1-cre*)1Jdun/J
CD-1 IGS albino mice	Charles River	CD-1 IGS, strain 022
mice with loxP sites flanking *Vps34* (*Pik3c3*) exon 17	Gift of Fan Wang, Duke U, described in Zhou et al.[27]	*Vps34*$^{fl/fl}$ Pik3c3$^{tm1.1Fawa}$
Vps34$^{fl/fl}$ Pik3c3mice on C57BL/6J background	> 6 generation back-crossing at BCM	
Knockin mice expressing low levels of human-rhodopsin-EGFP	BCM, described in Chan et al.[39]	hRhoG(H)
Other genotypes, as described in text and figures, were generated by crosses of strains listed above.		

(*Continued on next page*)

Continued

REAGENT or RESOURCE	SOURCE	IDENTIFIER
For all mouse strains, The absence of Pde6b^{rd1} was confirmed by PCR[68]; absence of Crb1^{rd8} was confirmed by PCR and sequencing of the relevant Crb1 region.[69]		
Committee Approving Studies		
Animal studies were approved by the Institutional Animal Care and Use Committee at Baylor College of Medicine.		
Oligonucleotides		
5′-ATGAACCTGGCGAGCCAGAGCG GAGAGGCC-3′ and 5′-GTCAGTCGGA GAATCATGGGAGGATGTTCGCTGT-3′ Primers for WIPI2 cloning		
5′- ATGCCCAAGAAGAAGAGGAAGGTG TCC -3′ and 5′- TGGCCCAAATGTTGCT GGATAGTTTTTA -3′ Primers for Best1-Cre genotyping		
hRho-GFP genotyping primers: 5′-GTTCCGGAACTGCATGCTCACCAC-3′ 5′-GGCGCTGCTCCTGGTGGG-3′		
Vps34 genotyping primers: A1, 5′-GGCCACCTAAGTGAGTTGTG-3′ A2, 5′-GAAGCCTGGAACGAGAAGAG-3′ A3, 5′-ATTCTGCTCTTCCAGCCACTG-3′		
Hrs cloning primers: 5′-ATGGAAAGTGATGCC ATGTTCGCTGCTGAAAG-3′ 5′-TGCCTTCTTGTTCAGCTGCTCATAG-3′		
Recombinant DNA		
Hepatocyte growth factor-regulated tyrosine kinase substrate (Hrs, GenBank: AAH03239.1) phosphoinositide-binding domain (amino acids 147-223) was cloned from purified C57BL/6 mouse kidney mRNA as described, He et al.[29]		GenBank: AAH03239.1
Mouse tandem PH domain-containing protein-1 (TAPP1) PH domain cDNA (amino acids 181-300), Dowler et al.[70] was a gift from Dario R. Alessi (University of Dundee, Scotland, U.K.);		
phospholipase C δ1 (PLCδ) PH domain (amino acids 1-175), Stauffer et al.[71] was a gift from Tobias Meyer (Addgene plasmid #21179).	Addgene	#21179
The sequence of four-phosphate-adaptor protein 1 (FAPP1) PH domain was identical to amino acids 1-100 of human FAPP1 (GenBank: AF286162.1);		GenBank: AF286162.1
inhibitor of growth protein-2 (ING2) cDNA was a gift from Curtis Harris (Addgene plasmid # 13294) Pedeux et al.[72]	Addgene	# 13294
WD repeat domain phosphoinositide-interacting protein 1 (WIPI1) cDNA was a gift from Noboru Mizushima (Addgene plasmid # 38272) Itakura et al.[73]	Addgene	# 38272

(*Continued on next page*)

Continued

REAGENT or RESOURCE	SOURCE	IDENTIFIER
Mouse WD repeat domain phosphoinositide-interacting protein 2 (WIPI2) cDNA was cloned from mouse retina phage cDNA (λZAPII) library (a gift from Wolfgang Baehr, University of Utah) using primers 5′-ATGAACCTGGCGAGCCAGAGCGG AGAGGCC-3′ and 5′-ACAGCGAACATCCTCCCATGATT CTCCGGACTGAC-3′, and the sequence was confirmed as identical to NM_178398.4.		NM_178398.4
Two tandem copies of Hrs, FAPP1, or TAPP1, three tandem copies of ING2, or one copy of PLCδ phosphoinositide-binding domains, or WIPI1 or WIPI2 cDNA were cloned with N-terminal EGFP or DsRed fusions in pCAG vector (a gift from Connie Cepko (Addgene plasmid #11150)) Matsuda & Cepko,[42] using EcoRI and NotI sites. All constructs were verified by sequencing.	Addgene	#11150
Software and algorithms		
ImageJ	NIH, Schindelin et al.[74]	https://imagej.nih.gov/ij/
Photoshop v.22	Adobe	
Mathematica v.11	Wolfram	
Origin version 10.2.3	Origin Lab	
Graphpad Prism 9.0	Graphpad Software, Inc.	

EXPERIMENTAL MODEL AND STUDY PARTICIPANT DETAILS

Mice

All animal studies were conducted according to NIH guidelines and approved by the Institutional Animal Care and Use Committee at Baylor College of Medicine. Wild-type C57BL/6J, B6 albino (B6(Cg)-Tyrc-2J/J), and transgenic mice that express Cre recombinase under control of the human bestrophin-1 (BEST1) promoter (C57BL/6-Tg(BEST1-cre)1Jdun/J, common name, Best1-cre, Strain #:017557)[51] were purchased from Jackson lab (Bar Harbor, ME). CD-1 IGS mice were purchased from Charles River (Wilmington, MA). Vps34 floxed mice, which have lox P sites flanking exons 17 and 18 (encoding the ATP binding domain),[27] were a gift from Fan Wang (Duke University). Vps34 floxed (Fl/Fl) mice were back-crossed to C57BL/6 for at least 6 generations and bred with the Best1-Cre mice to generate RPE-specific conditional functional Vps34 knockout mice (ΔRPE). The B6 mice were crossed with Vps34 knockout mice to obtain albino Vps34 floxed and Vps34ΔRPE. Vps34 knockout mice that were also heterozygous for the human rhodopsin-GFP allele at the mouse rhodopsin locus (ΔRPE/RG) were generated by crossing Vps34ΔRPE mice with human rhodopsin-GFP knock-in mice (hrhoG(H)) containing a lox H site in the 5′ non-coding region to reduce the human rhodopsin-GFP expression.[39] Confirmation of knockout was by staining RPE with Cre-reactive antibodies and assessing obvious phenotypes, including loss of PI(3)P puncta, tight junction disruption, loss of RPE65 expression, and accumulation of markers for autophagosomes, lysosomes and phagosomes, as detailed in Results. All of these were observed as early as 1 months PN, and at all later ages tested.

Mice used for tissue samples were euthanized by CO_2 inhalation prior to dissection following American Association for Laboratory Animal Science protocols. All the mice were maintained in a 12/12-hour light (400 Lux)/dark cycle. Tail DNA was used for Vps34 allele genotyping as described.[27] PCR primers 5′- ATGCCCAAGAAGAAGAGGAAGGTGTCC -3′ and 5′- TGGCCCAAATGTTGCTGGAT AGTTTTTA -3′ were used for PCR analysis of the Best1-Cre transgene.[51] The absence of Pde6b^{rd1} was confirmed by PCR[68]; absence of Crb1^{rd8} was confirmed by PCR and sequencing of the relevant Crb1 region.[69]

RPE cell cultures and treatment

ARPE-19 (CRL-2302; ATCC, Manassas, VA) were cultured in Corning DMEM/Ham's F-12 1:1 mixture (Fisher Scientific, Waltham, MA) with 10% FBS (Sigma, St. Louis, MO) and 10 μg/mL hygromycin B (ThermoFisher) were maintained at 37°C in 5% CO2.

ARPE-19 cells used in phagocytosis assays were cultured in as above but with 10% heat-inactivated FBS. The ARPE-19 cells used in all experiments were cultured for less than 20 passages.

Drug treatments were: 25 μg/mL chloroquine diphosphate salt (C6628), purchased from MilliporeSigma or 20 μM Vps34IN1 (S7980; Selleckchem, Houston, TX). Overnight drug treatments were for 12 hours, and acute treatments were for times as indicated. Control cells were treated with an equal volume of MQ water (for chloroquine) or DMSO (Vps34IN1).

METHOD DETAILS

Transfection

For the transfection experiments, cells were seeded in 24-well plates with coverslips. Next, 0.4 μg DNA, 2 μL ViaFect™ (Promega, Madison, WI) or 1.5 μL Lipomaster 3000 (Vazyme, Nanjing, PRC) and 40 μL Gibco Opti-MEM reduced serum media (Fisher Scientific) were mixed well and incubated at room temperature for 15 min, then added into each well containing 0.5 mL culture medium.

Mouse photoreceptor outer segment isolation

POS were purified from 2-month-old heterozygous human rhodopsin-EGFP knock-in mice as described.[75] The mice were dark-adapted overnight, and retinas were collected into 300 μL of 8% OptiPrep (Sigma) in Ringer's solution, vortexed at low speed for 2 min at room temperature under dim red light, and centrifuged at 400 x g at room temperature for 2 min. The supernatant containing mouse POS was collected and the retina pellet was extracted an additional 3-4 times with 8% Optiprep. The crude POS were loaded onto the top of a stepwise OptiPrep gradient (10%, 15%, 20%, 25% and 30%), and the gradient was centrifuged for 60 min at 24,700 $\times$ *g* at 4°C using a TLS-55 swinging bucket rotor (Beckman Coulter). Purified mouse POS were resuspended in DMEM/Ham's F-12 containing 2.5% sucrose. The concentration of the POS particles was estimated by Z1 Counter® Particle Counter (Beckman Coulter), and stored in the dark at −80°C.

In vitro phagocytosis

The phagocytosis assay was based on a previously reported protocol,[76] with modifications. POS were treated with 1 μM MFG-E8 and 0.1 μM Gas6 (R&D Systems) in DMEM/Ham's F-12 medium at room temperature for 30 min. ARPE-19 cells cultured on coverslips in a 24-well plate were treated with 20 μM Vps34-IN1 or the same volume of DMSO for 90 min, then were challenged with ~10-20 treated POS particles per cell for 2-4 hours at 37°C in a CO_2 incubator. The phagocytosis assay was terminated by washing the cells with ice-cold PBS-CM (PBS containing 1 mM $MgCl_2$ and 0.2 mM $CaCl_2$) 4-5 times. The cells were fixed with 4% paraformaldehyde in PBS for 15 min at room temperature, blocked with 1% BSA in PBS-CM for 30 min, then incubated with rabbit anti-LC3A/B at 1:100 dilution in blocking solution at room temperature for 1 hour, followed by donkey anti-rabbit Alexa Fluor 555, 2 μg/mL, and 300 nM DAPI in blocking solution for 1 hour at room temperature. The coverslips were washed 5 times with PBS-CM and mounted with Prolong Gold (Thermo).

Fluorescence microscopy

Samples were imaged with a Leica TCS SP5 confocal microscope using a Leica 63x oil immersion objective (HCX PL APO CS 63.0x, aperture1.40 oil) with lasers: diode 405, argon 488, HeNe 543, and HeNe 633. ImageJ was used for converting the original images to tiff files and contrast and brightness were adjusted in Photoshop (Adobe).

Fluorescence imaging of cultured cells

Transfected ARPE-19 cells were cultured in 24-well plates with #1.5 coverslip overnight, then fixed with 2% paraformaldehyde in PBS for 15 min at room. The fixed cells were incubated in blocking solution containing 5% donkey serum, 2.5% BSA, 0.2% fish gelatin, and 0.2% Triton X-100 in PBS at room temperature for 30min. The cells were incubated with primary antibodies diluted 1:50-1:100 with blocking solution at room temperature for 1 hour. After washing with PBS, the cells were incubated with secondary antibody conjugated with 2 μg/mL Alexa dye (Thermo) and 300 nM DAPI (Sigma) in blocking solution for 1 hour at room temperature, washed with PBS and mounted with prolong gold antifade mounting medium (Thermo).

For live-cell imaging, ARPE-19 cells were transfected with GFP-nxHrs or indicated plasmid DNAs in 24-well plates overnight, then transfected ARPE-19 cells were seeded in Lab-TeK II 8-chambered coverglass (Nunc, Rochester, NY) for 24 hours, then recorded at room temperature with Leica TCS SP5 confocal microscope using a Leica 63x oil immersion objective. The media was replaced with fresh DMEM/Ham's F-12 (without phenol red) containing 20 μM Vps34-IN1 or an equal volume of DMSO, and cells were imaged at 5 min intervals for 60 min.

In vivo plasmid electroporation

Sub-retinal injection and electroporation: pCAG-GFP or pCAG-GFP-2xHrs plasmid DNA (2 mg/mL) was introduced to the RPE by sub-retinal injection and electroporation of P0-P1 WT CD1, albino Vps34 floxed, or albino Vps34ΔRPE mice as described,[42,77] except that the electrodes were reversed such that the RPE, rather than the neural retina, was electroporated. Mouse pups were anesthetized, and the future edge of the eyelid was opened with an incision. A pilot hole was made with a 30-G beveled needle, a 33-G blunt needle was positioned in the subretinal space, and ~450 nL of plasmid DNA in PBS with 0.1% Fast Green dye was injected using a UMP3 Microsyringe Injector and Micro4 Controller (World Precision Instruments). Five square wave pulses (80 V,

50 ms with 950 ms-intervals) were applied with an ECM 830 square wave electroporator (BTX Harvard Apparatus) and custom tweezer-type electrodes, with the negative electrode on the injected eye. The injected eyes were collected for imaging after 4 weeks.

Immunofluorescence staining and fluorescence imaging of mouse RPE

Albino mice were dark-adapted for 12 h, then exposed to room light before they were sacrificed. Mouse eyes were excised and rinsed with PBS. The eyes were fixed with 4% paraformaldehyde in PBS for 45 min at room temperature then cryoprotected with 26% sucrose in PBS at 4°C overnight and embedded in optimum cutting temperature (O.C.T.) compound for sectioning. For flat-mount eyecup preparations, eyes were fixed with 4% paraformaldehyde in PBS for 45 min at room temperature, then washed with PBS 5-6 times; the cornea, iris, lens, and retina were removed, and eight symmetric radial cuts were made. RPE flat-mounts or eyecup sections were washed with PBS, then incubated in blocking solution (10% donkey serum, 5% BSA, 0.4% fish gelatin, and 0.4% Triton X-100 in PBS) at room temperature for 1 hour. The samples were incubated with primary antibodies diluted 1:50-1:100 with blocking solution at room temperature overnight. After washing with PBS, the samples were incubated with secondary antibody conjugated with 2 μg/mL Alexa dye (Thermo) and 300 nM DAPI (Sigma) in blocking solution for 1 hour at room temperature, washed with PBS and mounted with VECTASHIELD antifade mounting medium (Vector Laboratories).

Tiled images of flat-mount RPE were acquired with the ZEISS Apotome2 Microscope system (Zeiss, Oberkochen, Germany) with 40x water immersion objective. Each tile was 1024 x 1024 with pixel size 6.45 $\times$ 6.45 μm, and ~350-400 tiles were stitched together using ZEN 2 (blue edition) software (Zeiss). Raw images scaled to 3.23 μm/pixel were used for automated detection of p62 puncta using the "MorphologicalComponents" function in Mathematica (Wolfram), with the "ConvexHull" method and background value of 0.3. Very large features (containing $\geq$ 500 px), resulting from imaging artifacts at the edges of the tissue, were omitted from the data set. Flat-mount areas were determined in ImageJ from regions of interest drawn manually along the borders of the tissue.

Analysis of fluorescence intensities was performed using ImageJ and GraphPad Prism (version 10.2.3) software. The integrated fluorescence intensity within a boxed Region of Interest (ROI), was recorded, and the fluorescence intensities of ROI within the Vps34 KO RPE images were divided by the intensities of ROIs of the same size in comparable regions of control RPE images to normalize the fluorescence intensity within each group of mice.

Statistical analysis of images

All comparisons were between images with all parameters identical except for the genotype. Pairwise comparisons were carried out using Student's *t*-test with *p* values less than 0.05 considered as significantly different. Plotted values are means ± sample standard deviation.

Transmission electron microscopy (TEM)

Transmission Electron Microscopy (TEM) was performed as described.[29] Eye cups were fixed with 3% paraformaldehyde and 3% glutaraldehyde solution in 0.1M cacodylate buffer, pH 7.4 (CB) for 1-3 days at 4°C. Eyecups were washed, post-fixed with 1% OsO4 in 0.1M CB for 1 hour, and dehydrated by sequential incubation in 30%, 50%, 70%, 85%, 90%, and 100% ethanol. The tissue was incubated with several changes of acetone and gradually infiltrated with 2:1, 1:1, and 1:2 acetone to resin (Embed-812, Electron Microscopy Sciences, Hatfield, PA) mixtures, followed by pure resin for 48 h. Resin blocks were polymerized at 60°C for 24-48 hours. 80-90 nm sections were cut on a Leica Ultracut UCT microtome, collected on 50 or 75 mesh grids and stained with 2% uranyl acetate and Reynold's lead citrate. Images were taken on a Zeiss transmission electron microscope equipped with a CCD camera (Advanced Microscopy Techniques Corp., Woburn, MA).

Cloning of DNA constructs

Hepatocyte growth factor-regulated tyrosine kinase substrate (Hrs, GenBank: AAH03239.1) phosphoinositide-binding domain (amino acids 147-223) was cloned from purified C57BL/6 mouse kidney mRNA as described.[29] GFP-2xHRS cDNA was subcloned into pCAG vector using EcoRI and NotI sites.[29] For pCAG GFP-3x and 4x HRS constructs, BamHI site in the linker between 2 HRS domains was mutated into KpnI site, then additional HRS cDNAs were inserted into KpnI site. To generate GST fusion expression constructs, 2x, 3x and 4x tandem copies of HRS cDNAs were subcloned into NdeI and EcRI sites in pGEX vector. GST-1D4 cDNA was subcloned into pET14b vector using NcoI and BamHI sites.

Mouse tandem PH domain-containing protein-1 (TAPP1) PH domain cDNA (amino acids 181-300)[70] was a gift from Dario R. Alessi (University of Dundee, Scotland, U.K.); phospholipase C δ1 (PLCδ) PH domain (amino acids 1-175)[71] was a gift from Tobias Meyer (Stanford University, CA); The sequence of four-phosphate-adaptor protein 1 (FAPP1) PH domain was identical to amino acids 1-100 of human FAPP1 (GenBank: AF286162.1); inhibitor of growth protein-2 (ING2) cDNA was a gift from Curtis Harris (Addgene plasmid # 13294)[72]; and WD repeat domain phosphoinositide-interacting protein 1 (WIPI1) cDNA was a gift from Noboru Mizushima (Addgene plasmid # 38272).[73] Mouse WD repeat domain phosphoinositide-interacting protein 2 (WIPI2) cDNA was cloned from mouse retina phage cDNA (λZAPII) library (a gift from Wolfgang Baehr, University of Utah) using primers 5′-ATGAACCTGGCGAGCCAGAGCGGAGAGGCC-3′ and 5′-ACAGCGAACATCCTCCCATGATTCTCCGGACTGAC-3′, and the sequence was confirmed as identical to NM_178398.4. Two tandem copies of Hrs, FAPP1, or TAPP1, three tandem copies of ING2, or one copy of PLCδ phosphoinositide-binding domains, or WIPI1 or WIPI2 cDNA were cloned with N-terminal EGFP or DsRed fusions in pCAG vector (a gift from Connie Cepko, Addgene plasmid #11150)[42] using EcoRI and NotI sites. All constructs were verified by sequencing.

Expression and purification of phosphoinositide binding proteins

GST-2xHrs-1D4, GST-3xHRS-1D4, GST-4xHRS-1D4, and GST-1D4 were expressed in BL21(DE3)pLysS E. coli (MilliporeSigma, Burlington, MA). Transfected cells were grown at 20°C for 3 hours following induction with 1mM isopropyl β-D-1-thiogalactopyranoside (IPTG). The cells were harvested, and the cell pellet was resuspended with 40mM Tris, pH 7.6, 0.2M NaCl, 5mM DTT, 1% Triton x-100, phenylmethanesulfonyl fluoride (PMSF) and cOmplete™ Protease Inhibitor Cocktail without EDTA (Sigma), then lysed using a sonicator (Fisher, 550 Sonic dismembrator). The insoluble cellular debris was removed by centrifugation for 30 min at 13,865 $\times g$ at 4°C using a JA25.50 rotor (Beckman Coulter). Protein purification was performed with Glutathione Sepharose 4 Fast Flow (GE Healthcare) following the manufacturer's protocol. Before the GST fusion proteins were eluted from the column, the detergent was washed out with 40 mM Tris, pH 7.6, 0.2 M NaCl, 5 mM DTT, then eluted with 40 mM Tris, pH 7.5 and 40 mM reduced L-Glutathione (Sigma). Purified proteins were dialyzed against 40 mM Tris pH 7.5, 150 mM NaCl, and PMSF at 4°C overnight, then supplemented with 50% glycerol and PMSF, and stored at −20°C. The protein concentration was determined using Bradford assay reagent (Bio-Rad).

Phosphoinositide ELISA assay

The phosphoinositide ELISA assay[57] was modified for determination of PI(3)P binding to purified GST-nxHrs-1D4. Synthetic PI(3)P diC16 standard (P-3016), DPPC (L1116), DPPS (L3116) and DOPE (L2182) were purchased from Echelon Biosciences (Salt Lake City, UT). PI(3)P diC16 (5 pmol to 39 pmol) was mixed with 100 pmol PC:PE:PS = 50:35:15 (molar ratio) in 40μL methanol:chloroform (9:1 v/v) and the mixture was added into the wells of black PolySorp 96-well plates (Thermo Fisher, 437112). The lipids were air-dried and then dried under vacuum overnight. Each plate was blocked with 5% BSA (Sigma) in PBS for 3 hours at room temperature and then incubated with 100 μL/well of 30 nM purified either GST-1D4, GST-2xHRS-1D4, GST-3xHRS-1D4 or GST-4xHRS-1D4 in PBS containing 3% (w/v) BSA in at 4°C overnight. The plates were then incubated with monoclonal 1D4 antibody at 1 μg/ml in PBS with 3% BSA at room temperature for 3 hours followed by washing with PBS 8 times. Wells were then incubated with 1:3,000 diluted goat anti-mouse-HRP (Thermo) in PBS with 3% BSA at room temperature for 1 hour. After washing with PBS, the plates were incubated with 100 μL/well of SuperSignal ELISA Femto Maximum Sensitivity Substrate (Thermo) at room temperature for 1 min, and the chemiluminescence signals were detected using a FlexStation 3 (Molecular Devices). The assays were repeated more than 3 times. The statistical analysis of the data was carried out using Origin software.

QUANTIFICATION AND STATISTICAL ANALYSIS

ELISA assays using chemiluminescence signals measured on a FlexStation 3 (Molecular Devices) were repeated more than 3 times. The statistical analysis of the data was carried out using Origin software. Data were subjected to non-linear least-squares fit to the equation: $Luminescence = L0 + Lmax(\text{pmol of PI(3)P}/(\text{pmol of PI(3)P} + k)$ using the Levenberg-Marquardt algorithm. Standard deviations of the fits calculated by the variances determined automatically in that algorithm were used to determine statistical significance by Students *t*-test.

Statistical analysis of images

All comparisons were between images with all parameters identical except for the genotype. Within ImageJ, the integrated fluorescence intensity within a boxed Region of Interest (ROI), was recorded, and the fluorescence intensities of ROI within the Vps34 KO RPE images were divided by the intensities of ROIs of the same size in comparable regions of control RPE images to normalize the fluorescence intensity within each group of mice. Pairwise comparisons were carried out in GraphPad Prism (version 10.2.3) using Student's *t*-test with p values less than 0.05 considered as significantly different. Plotted values are means ± sample standard deviation.